THE CELLULAR UPTAKE OF LUMINESCENT RUTHENIUM COMPLEXES

Thesis by

Cindy A. Puckett

In Partial Fulfillment of the Requirements

for the Degree of

Doctor of Philosophy in Chemistry

California Institute of Technology

Pasadena, California

2010

(Defended October 28, 2009)

ACKNOWLEDGEMENTS

I must first acknowledge my research advisor, Professor Jacqueline Barton, without whom none of this work would have been possible. I appreciate the support and encouragement you have provided me over the years. I also thank you for bringing together such an intelligent group of people who are always eager to help each other out. I have a learned a great deal in your lab—Thank you for making me a chemist.

My journey to Caltech would not have happened without the guidance from my undergraduate professors. I thank Professor Jeffrey Charonnat for getting me started in chemistry research and helping me with the transition to graduate school.

I would like to express my appreciation for my faculty committee, Professors Dennis Dougherty, Nate Lewis, and Doug Rees, for all of their feedback and suggestions.

I was fortunate to work with a wonderful collaborator, Professor Nick Turro, who led me briefly but fruitfully into the world of molecular beacons.

I owe many thanks to Maureen Renta, who works extraordinarily hard to keep the Barton group running smoothly. I appreciate her advice, assistance, and humor. I am also indebted to Shelley Diamond of Caltech's Flow Cytometry Facility for her generous assistance with my research.

Many members of the Barton group, past and present, deserve much thanks for their help and support: Anne Petitjean, Jon Hart, and Irv Lau for getting me started in the group; Fangwei Shao for her great sense of humor; Jens Brunner, for synthetic assistance on peptide couplings; Valerie Pierre, for her friendship and advice; Marisa Buzzeo, for

guidance; Mi Hee Lim, for her synthetic expertise; Amie Boal, for advice and sharing her tasty fruit pies; Brian Zeglis, for his willingness to donate compounds and organizing numerous Barton group activities; Russ Ernst, for being a great cell culture room labmate and review collaborator; Hang Song, for her positive energy; Curtis Schneider, for helpful discussions on my proposals; Pam Sontz, for making the lab more fun; Jason Slinker, for hosting group get-togethers; Paul Lee and Wendy Mercer, for being good friends; and Eddie Merino, for advice, mentorship, and friendship.

I must also thank my friends Antek Ignatowicz and Diane Stucker, whom I could call at any time for moral support, and who kept me aware of life outside graduate school. Over the last couple years, I have had a terrific roommate, Erisa Hines, who is a source of encouragement and has not once protested Joey's constant presence at our apartment.

Another anchor throughout my graduate career was my family. I would like to thank my brother Roger for all his help, including setting up my apartment. I thank my parents for their support and providing me a place to relax. I also appreciate the family of Joey Genereux, especially Beverly, for their encouragement.

Finally, my love and thanks go to Joey Genereux. You are kind and generous. You have always been there for me. I cannot thank you enough.

ABSTRACT

Transition metal complexes have enormous potential as diagnostic and therapeutic agents, but their internalization and distribution in living cells are only poorly understood. Here, we perform one of the few systematic explorations of the uptake efficiency and mechanism of a class of metal complexes: luminescent dipyridophenazine (dppz) complexes of ruthenium(II). Substitution of the ancillary ligands permits variation in the overall complex charge, size, and hydrophobicity. We find that internalization of these complexes occurs mostly through passive diffusion, driven by the membrane potential, and that hydrophobicity, rather than size, is the most important determinant of compound accumulation. Across different cell types with all compounds, mostly uneven cytoplasmic staining is observed with near exclusion from the nucleus. Conjugation to cell-penetrating peptides, such as D-octaarginine, increases uptake efficiency, but leads to trapping in endosomes below a threshold concentration. Above this threshold concentration, substantial staining of the nucleus as well as the cytosol is observed. An appended fluorescein tag lowers the threshold concentration, indicating the importance of payload to the internalization and distribution of cell-penetrating peptides. Shorter peptides, including the nuclear targeting signal RrRK (where r = D-arginine), are also studied, though none have as high a degree of uptake nor as low a threshold concentration as the octaarginine conjugate. These studies provide a basis for the future design and optimization of metal complexes for biological application.

TABLE OF CONTENTS

LIST OF FIGURES AND TABLES

CHAPTER 1: METHODS TO EXPLORE THE CELLULAR UPTAKE OF LUMINESCENT RUTHENIUM COMPLEXES[†]

1.1: INTRODUCTION

1.1.1: SIGNIFICANCE OF UPTAKE

Transitional metal complexes are appealing candidates in the search for new diagnostic and therapeutic agents. They represent a uniquely modular system, wherein the metal center holds its ligands in a precisely defined three-dimensional structure. These ligands can be varied relatively easily, in order to selectively change the characteristics of the complex in either subtle or dramatic fashion. Transition metal complexes also offer rich photophysical and photochemical properties, expanding their utility beyond structural recognition.

Biological applications of transition metal complexes are increasingly being explored.[1–3] Currently, we are investigating 5,6-chrysenequinone diimine (chrysi) complexes of rhodium(III) as potential chemotherapeutic agents. These complexes target single base mismatches in DNA and selectively inhibit cellular proliferation in mismatch repair-deficient cell lines.[4–6] To be effective, these compounds must reach the intended location inside the cell.

The cell membrane represents a formidable barrier to this goal. Only molecules within a narrow range of molecular weight, charge, and polarity are typically able to directly cross the plasma membrane by passive diffusion.[7] Larger molecules are generally

[†] Parts of this chapter were adapted from Puckett, C. A.; Barton, J. K. Methods to explore cellular uptake of ruthenium complexes. *J. Am. Chem. Soc.* **2007,** *129,* 46–47.

internalized by endocytosis, a process that involves invagination of the plasma membrane to form a vesicle. However, molecules that enter by this route often fail to escape from these vesicles. Compounds that target genomic DNA must also bypass the nuclear membrane.

The cellular uptake properties of transition metal complexes are not well developed. The notable exception is cisplatin, whose cellular accumulation has been examined in detail and recently reviewed.[8] Also, Parker and coworkers have characterized the mechanism of uptake for several luminescent Eu(III) and Tb(III) complexes, and found that they enter cells by endocytosis (specifically macropinocytosis).[9] Generally, studies of metallocomplexes have revealed that they are as diverse in their uptake properties as organic and biomolecular compounds. Here, we apply a broad spectrum of techniques to explore the uptake and distribution of ruthenium(II) polypyridyl complexes, which serve as luminescent analogues of our rhodium therapeutics.

1.1.2: METHODS TO EXAMINE CELLULAR ACCUMULATION OF METAL COMPLEXES

Metal complexes for diagnostic applications are frequently luminescent, allowing ready characterization of their uptake characteristics. They can be examined by fluorometry, confocal microscopy,[3] and flow cytometry.[10] For non-luminescent complexes, inductively coupled plasma mass spectrometry (ICP-MS),[11,12] atomic absorption spectroscopy (AAS),[13] and UV-visible absorption spectroscopy[14] are used.

Prior to ICP-MS, AAS, UV-visible absorption spectroscopy, and fluorometry

measurements, cell lysates are prepared from cells that have been incubated with metal complex. When adherent cells are used, they are either detached from the culture dish and then lysed, or lysed directly in the dish. Alternatively, the cells can be detached and treated with complex in suspension, though in this case, the cells are not in their normal growing environment. This cell lysate is analytically diluted, and the amount of metal in the solution is quantified. Amounts are typically reported versus cell number or total protein concentration. Independent of the quantification technique, attention must be paid to certain steps to ensure accurate results. Egger and colleagues have found that adsorption to the culture plates and sample storage conditions prior to analysis significantly influence recovery of the metal.[11] Factors affecting adsorption include concentration of the complex, the amount of protein in the medium, the duration of contact of protein-containing medium before treatment with complex, and the lipophilicity of the complex. Adsorption-related artifacts are particularly an issue when lysis is performed directly in the culture dishes. To correct for these effects, adsorption blanks of cell-free samples treated with metal complex should be performed. A second major issue is the time that the sample is stored prior to measurement, as the recovery of analyte decreases with time. Consequently, samples should be quantified immediately after preparation. When these considerations are taken into account, reliable measurements of metal complex uptake can be performed.

The cellular uptake of luminescent metal complexes are primarily examined using two complementary methods, flow cytometry and confocal microscopy; fluorometry of cell lysates can also be performed. For flow cytometry, cells are detached from culture

either before or after incubation with the metal complex to produce a cell suspension. Untreated cells are used for the autofluorescence control. To exclude dead cells from analysis, a membrane-impermeable dead cell dye, such as propidium iodide, can be added.[15] The cells are inspected individually as they pass single file through the laser beam(s) and the instrument records their light scatter and luminescence. Optical band pass filters separately collect the emission from multiple fluorophores. The result is a distribution of luminescence for the cell population, which can be depicted as a histogram of luminescence intensity versus the number of cells. The luminescence intensity of different cell populations, e.g., treated with different complexes or different incubation conditions, is easily compared.

Flow cytometry is faster and less labor intensive than preparation of samples for ICP-MS. It also provides a distribution of cellular uptake, rather than only the mean uptake of all the cells. Samples prepared for flow cytometry will have the same adsorption issues described above, though they may be less significant, as the cells are detached from the culture dish after incubation with the metal compound, rather than lysed in the dish, or incubated in suspension following detachment. Flow cytometry distinguishes live from dead cells by uptake of a dead cell dye, whereas with ICP-MS, dead cells are eliminated from analysis if they have lost adherence to the culture dish and are washed away before the lysis step. Both techniques have their purpose, as ICP-MS provides absolute values for uptake, while flow cytometry is limited to luminescent compounds and is better suited for comparing the amount of uptake under different conditions.

Flow cytometry and analysis of cell lysates by ICP-MS and other methods only provide a measurement of the total amount of metal complex associated with the cell; they do not distinguish between membrane-bound and intracellular material. Localization is difficult to discern by these techniques, where cellular components, such as nuclei, must be physically isolated before the metal content can be determined.

Confocal microscopy, on the other hand, reveals the spatial distribution of luminescent metal complexes inside the cell. Co-staining with organelle dyes can be performed to further pinpoint their intracellular location. Another notable advantage of microscopy over ICP-MS is that lesser amounts of metal complex are typically required, as the incubations can be performed in small wells (e.g., those of a 96-well plate). To acquire better quality images, adherent cells are preferable over suspension cells, and the cells should not be confluent. Importantly, cells should be imaged live rather than fixed, as fixation can cause artifactual redistribution of compounds.[16] In all the uptake experiments, attention should be paid to the number of cells incubated with the metal complex, since the amount of uptake may be dependent on it. This has been shown to be the case for cell-penetrating peptides.[17]

1.2: EXPERIMENTAL PROTOCOLS

1.2.1: MATERIALS AND INSTRUMENTATION

Media, cell culture supplements, and TO-PRO®-3 iodide were purchased from Invitrogen (Carlsbad, CA). $RuCl_3$ was purchased from Pressure Chemical Co (Pittsburgh, PA). 2,2′-bipyridine (bpy), 1,10-phenanthroline (phen), 4,4′-dimethyl-2,2′-bipyridine, and

3,4,7,8-tetramethyl-1,10-phenanthroline (Me_4phen) were obtained from Sigma-Aldrich (St. Louis, MO). 4,7-diphenyl-1,10-phenanthroline (DIP) was purchased from GFS Chemicals (Columbus, OH). Calf thymus (CT) DNA was purchased from Amersham Biosciences, GE Healthcare (Pittsburgh, PA). All commercial materials were used as received.

^{1}H NMR spectra were recorded on a 300 MHz Varian spectrometer. Mass spectrometry was performed at either the Caltech mass spectrometry facility or in the Beckman Institute Protein/Peptide Micro Analytical Laboratory. Absorption spectra were recorded on a Varian Cary 100 or Beckman DU 7400 spectrophotometer. Unless otherwise referenced, extinction coefficients of Ru complexes were determined using inductively coupled plasma mass spectrometry (ICP-MS). Luminescence measurements were performed on an ISS K2 fluorimeter equipped with a 300 W xenon lamp as an excitation source. HPLC was performed on an HP1100 system equipped with a diode array detector using a Vydac C_{18} reversed-phase semipreparative column.

1.2.2: RU COMPLEX SYNTHESIS

Dipyrido[3,2-*a*:2′,3′-*c*]phenazine (dppz) and 4′-methyl-2,2′-bipyridine-4-carboxylic acid (mcbpy) were prepared according to previously recorded procedures.[18,19] 4-Aminomethyl-4′-methyl-2,2′-bipyridine (NH_2-bpy) was prepared from 4,4′-dimethyl-2,2′-bipyridine as described by Berg et al. (to make 4-hydroxymethyl-4′-methyl-2,2′-bipyridine) and Hamachi et al.[20,21]

1.2.2.1: SYNTHESIS OF 4-ETHOXY-4′-METHYL-2,2′-BIPYRIDINE (CO_2ET-BPY)

4′-methyl-2,2′-bipyridine-4-carboxylic acid (111 mg) was refluxed in 10 mL ethanol with conc. H_2SO_4 (10 drops). Reaction progress was complete by 8 h, as monitored by TLC (silica, 5% methanol in CH_2Cl_2). The mixture was cooled to 0 °C and neutralized with saturated $NaHCO_3$, then concentrated *in vacuo*. Water was added, and the solution was extracted with CH_2Cl_2. The organic layer was washed with water, dried with Na_2SO_4, filtered, and concentrated *in vacuo*. The pale yellow solid was purified on a silica column using 1:1 ethyl acetate:hexanes to yield a white solid. ^{1}H NMR (acetone-d_6, 300 MHz): δ 8.98 (m, 1H), 8.86 (dd, 1 H, 5.0 Hz, 1.1 Hz), 8.57 (m, 1H), 8.34 (m, 1H), 7.89 (dd, 1 H, 5.0 Hz, 1.7 Hz), 7.30 (dd, 1 H, 5.0 Hz, 1.1 Hz), 4.45 (q, 2H, 7.1 Hz), 2.47 (s, 3H), 1.42 (t, 3H, 7.1 Hz).

1.2.2.2: SYNTHESIS OF 4-NH-FMOC-4′-METHYL -2,2′-BIPYRIDINE

4-Aminomethyl-4′-methyl-2,2′-bipyridine (45 mg, 0.23 mmol) was dissolved in 3 mL CH_2Cl_2. 9-Fluorenylmethoxy-carbonyl-N-hydroxysuccinimide (Fmoc-OSu) (114 mg, 0.34 mmol), dissolved in 3 mL CH_2Cl_2, was added. After 2 h, 59 μL DIEA was added, and the mixture was stirred under $Ar_{(g)}$ for 29 h. The solution was rinsed twice with saturated sodium bicarbonate. The dichloromethane solution was dried with magnesium sulfate, filtered, and concentrated *in vacuo*. The product was purified by silica column (pre-treated with 90:10 hexanes:triethylamine), eluting with 1:1 ethyl acetate:hexanes followed by ethyl acetate. A white solid was obtained. ESI-MS (cation): 422.2 *m/z* ($M^+ + H^+$) obsd, 422.2 *m/z* ($M^+ + H^+$) calcd. ^{1}H NMR ($CDCl_3$, 300 MHz):

δ 8.62 (d, 1H, 5.1 Hz), 8.53 (d, 1H, 5.1 Hz), 8.30 (s, 1H), 8.23 (s, 1 H), 7.77 (d, 2H, 7.5 Hz), 7.61 (d, 2H, 7.5 Hz), 7.41 (m, 2H), 7.31 (m, 2H), 7.19 (d, 1H, 5.1 Hz), 7.15 (d, 1H, 3.6 Hz), 5,23 (broad s, 1H), 4.49 (m, 4H), 4.25 (t, 1H, 6.6 Hz), 2.45 (s, 3 H).

1.2.2.3: SYNTHESIS OF $[RuL_2DPPZ]Cl_2$; L = 2,2′-BIPYRIDINE (BPY), 1,10-PHENANTHROLINE (PHEN), OR 4,7-DIPHENYL-1,10-PHENATHROLINE (DIP)

$Ru(bpy)_2Cl_2$ was synthesized as previously described.[22] $Ru(DIP)_2Cl_2$ and $Ru(phen)_2Cl_2$ were synthesized in an analogous fashion to $Ru(bpy)_2Cl_2$. The dipyridophenazine (dppz) ligand was added to RuL_2Cl_2 by refluxing in ethanol-water for > 3 h to make $Ru(DIP)_2dppz^{2+}$ and $Ru(phen)_2dppz^{2+}$. The ethanol was removed under vacuum, resulting in precipitation of $[Ru(DIP)_2dppz]Cl_2$, which was collected by filtration. The compound was purified via room temperature recrystallization by diffusion of ether into acetonitrile. $Ru(phen)_2dppz^{2+}$ was precipitated from water as the hexafluorophosphate salt, then returned to the chloride salt by Sephadex DEAE anion exchange column. The Ru complexes utilized are racemic mixtures of the two enantiomers. Ru complex concentrations were determined by UV/vis absorbance: $Ru(bpy)_2dppz^{2+}$, $\varepsilon_{444\ nm}$ = 16,100 M^{-1} cm^{-1};[24] $Ru(phen)_2dppz^{2+}$, $\varepsilon_{440\ nm}$ = 21,100 M^{-1} cm^{-1};[25] and $Ru(DIP)_2dppz^{2+}$, $\varepsilon_{433\ nm}$ = 34,300 M^{-1} cm^{-1}.

1.2.2.4: SYNTHESIS OF $[Ru(Me_4phen)_2dppz]Cl_2$

$Ru(Me_4phen)_2Cl_2$ was synthesized in a similar manner to $Ru(bpy)_2Cl_2$, except that the reaction time was shortened to 3 h (reaction for 8 h produces a larger amount of

impurities), and the reaction was performed under $Ar_{(g)}$ and protected from light. Dppz was added to $Ru(Me_4phen)_2Cl_2$ as described above to form $Ru(Me_4phen)_2dppz^{2+}$. The complex, as the PF_6^- salt, was first purified on a neutral alumina column, eluting with CH_3CN. The product was converted to the Cl^- salt by anion exchange chromatography (Sephadex DEAE). Further purification by HPLC yielded the complex in analytical purity. ESI-MS (cation): 428.2 *m/z* (M^{2+}) obsd, 428.1 *m/z* (M^{2+}) calcd. UV/vis (H_2O, pH 5): 269 nm (130,500 M^{-1} cm^{-1}), 358 nm (18,100 M^{-1} cm^{-1}), 376 nm (22,900 M^{-1} cm^{-1}), 422 nm (21,200 M^{-1} cm^{-1}).

1.2.2.5: SYNTHESIS OF $[Ru(CO_2Et\text{-}bpy)_2dppz]Cl_2$

$Ru(CO_2Et\text{-}bpy)_2Cl_2$ was synthesized according to the protocol of Leasure and coworkers,[23] except 2:1 dimethoxyethane:ethanol was used as the reaction solvent. The dppz ligand was added by refluxing in ethanol for 24 h. The complex was purified by a neutral alumina column eluting with CH_3CN, followed by recrystallization by slow diffusion of ether into CH_3CN. Complex was converted to the Cl^- salt by anion exchange chromatography (Sephadex DEAE). ESI-MS (cation): 433.9 *m/z* (M^{2+}) obsd, 434.1 *m/z* (M^{2+}) calcd. UV/Vis (H_2O, pH 5): 293 nm (110,000 M^{-1} cm^{-1}), 360 nm (28,700 M^{-1} cm^{-1}), 372 nm (28,200 M^{-1} cm^{-1}), 463 nm (29,300 M^{-1} cm^{-1}).

1.2.2.6: SYNTHESIS OF $Ru(mcbpy)_2dppz$

This complex was formed by hydrolysis of the ester. $[Ru(CO_2Et\text{-}bpy)_2dppz]Cl_2$ was suspended in 0.5 M LiOH and stirred overnight. The reaction mixture was

neutralized with 1 M HCl and desalted with a Sep-Pak C_{18} cartridge (Waters Chemical Co). A red-orange solid was obtained. ESI-MS (cation): 406.0 *m/z* (MH_2^{2+}), 416.9 *m/z* ($MNaH^{2+}$), 427.9 *m/z* (MNa_2^{2+}) obsd, 406.1 *m/z* (MH_2^{2+}) calcd. UV/Vis (H_2O, pH 5): 292 nm (100,200 M^{-1} cm^{-1}), 358 nm (25,400 M^{-1} cm^{-1}), 372 nm (24,600 M^{-1} cm^{-1}), 458 nm (25,400 M^{-1} cm^{-1}).

1.2.2.7: SYNTHESIS OF $[RU(NH_2\text{-}BPY)_2DPPZ]CL_2$

This complex was synthesized using the Fmoc-protected ligand, 4-NH-Fmoc-4′-methyl-2,2′-bipyridine. Preparation of $Ru(NH\text{-}Fmoc\text{-}bpy)_2Cl_2$ was accomplished using the method of Leasure and coworkers.[23] Dppz was added by refluxing in 1:1 ethanol:water for 7 h. The ethanol was removed *in vacuo*, and the water solution was filtered. $Ru(NH\text{-}Fmoc\text{-}bpy)_2dppz^{2+}$ was precipitated by addition of NH_4PF_6 to the filtrate, and converted to the chloride salt by anion exchange chromatography (Sephadex DEAE). Product was purified by HPLC.

Deprotection of $Ru(NH\text{-}Fmoc\text{-}bpy)_2dppz^{2+}$ to give $Ru(NH_2\text{-}bpy)_2dppz^{2+}$ was performed using 0.5% piperidine (v/v) in DMF for 15 min. Higher concentrations of piperidine (5%) produced impurities. The DMF/piperidine solution was removed *in vacuo*. The residue was dissolved in water, filtered, and the product was precipitated as the PF_6^- salt using NH_4PF_6. After rinsing carefully with water, the orange solid was dissolved in 1:1 acetonitrile:water and converted to the chloride salt by anion exchange chromatography (Sephadex DEAE). ESI-MS (cation): 391.1 *m/z* (M^{2+}) obsd, 391.1 *m/z*

(M^{2+}) calcd. UV/Vis (H_2O, pH 5): 286 nm (99,400 M^{-1} cm^{-1}), 359 nm (19,900 M^{-1} cm^{-1}), 371 nm (19,500 M^{-1} cm^{-1}), 458 nm (17,900 M^{-1} cm^{-1}).

1.2.3: CELL CULTURE

Cell lines were maintained in the following medium: minimal essential medium alpha with 10% fetal bovine serum (FBS), 100 units/mL penicillin, and 100 μg/mL streptomycin for HeLa (ATCC, CCL-2) and DU-145 (ATCC, HTB-81); McCoy's 5a medium with 10% FBS, 100 units/mL penicillin, and 100 μg/mL streptomycin for SKOV-3 (ATCC, HTB-77) and HT-29 (ATCC, HTB-38**)**; F-12K medium with 10% FBS 100 units/mL penicillin, and 100 μg/mL streptomycin for A-549 (ATCC, CCL-185); and RPMI medium 1640 supplemented with 10% FBS, 2 mM L-glutamine, 0.1 mM nonessential amino acids, 1 mM sodium pyruvate, 100 units/mL penicillin, 100 μg/mL streptomycin, and 400 μg/mL Geneticin (G418) for HCT116N and HCT116O. Cells were grown in tissue culture flasks at 37 °C under 5% CO_2 atmosphere.

1.2.4: FLOW CYTOMETRY

Cells were detached from culture with EDTA (0.48 mM in phosphate-buffered saline) and incubated at $1x10^6$ cells/mL with 10 μM ruthenium complex (added from a concentrated stock) in Hanks' Balanced Salt Solution (HBSS) supplemented with 2.5 mg/mL bovine serum albumin fraction V (BSAV) at 37 °C for 2 h, then rinsed with buffer and placed on ice. TO-PRO-3 was added at 1 μM immediately prior to flow cytometry analysis to stain dead cells. The fluorescence of ~20,000 cells was measured

using a BD FACS Aria at the Caltech Flow Cytometry Facility. Ruthenium complexes were excited at 488 nm, with emission observed at 600–620 nm. TO-PRO-3 was excited at 633 nm, with emission observed at 650–670nm. Cells exhibiting TO-PRO-3 fluorescence were excluded from the data analysis. For nuclei experiments, the nuclei buffer (vide infra) was used as the sheath fluid on the flow cytometer.

1.2.5: CONFOCAL MICROSCOPY

Cells used for microscopy were seeded on glass-bottom 96-well plates (Whatman) and allowed to attach overnight. For incubations shorter than 24 h, approximately 4000 cells were seeded. Longer incubations required that fewer cells be seeded to allow room for cell proliferation, e.g., for the cell line comparison experiments, 3000 cells were seeded. After incubation with the ruthenium complex in complete medium (containing 10% fetal bovine serum), cells were rinsed with Hanks' Balanced Salt Solution and imaged without fixation (unless otherwise noted). Images were collected on a Zeiss LSM 510 or Zeiss LSM 5 Exciter inverted microscope using a 63x/1.4 oil immersion objective at the Caltech Biological Imaging Center. Nuclei were examined using a 20x objective. The ruthenium complexes were excited at 488 nm, with emission observed using a long-pass 560 nm filter.

For the cell fixation experiments, HeLa cells were incubated with 5 μM $Ru(DIP)_2dppz^{2+}$ for 2 h at 37 °C. One well of cells was subsequently treated with cold methanol for ~ 3 min and rinsed with phosphate-buffered saline (PBS). A second well

was fixed with 2% formaldehyde for 5 min, then permeabilized with 0.1% Triton X-100 in PBS for 6 min.

1.2.6: ISOLATION OF NUCLEI

Cells were detached with trypsin (no EDTA) for 5 min at 37 °C. The cells were rinsed once with cold phosphate-buffered saline (PBS), then resuspended in cold nuclei extraction buffer (320 mM sucrose, 5 mM $MgCl_2$, 10 mM HEPES, 1% Triton X-100 at pH 7.4), giving approximately 1 mL per 1 million cells. The cell suspension was vortexed for 10 s and incubated on ice for 9 min. The nuclei were pelleted by centrifuged at 2000 g (~2950 rpm) for 4 min at 4 °C, washed twice with cold nuclei wash buffer (320 mM sucrose, $MgCl_2$, 10 mM HEPES at pH 7.4), and resuspended in cold nuclei wash buffer with vortexing. The solution was triturated 5–10 times with a 1 mL micropipette to break up clumps of nuclei, then filtered through a 35 μm cell strainer (BD Falcon) to remove any remaining clumps. The nuclei solution was stored on ice until analysis. Nuclei isolation was confirmed by examining an aliquot mixed with an equal volume of 0.4% Trypan blue (the nuclei stain blue). For confocal microscopy, nuclei were suspended in PBS prior to imaging.

The following control for contamination of nuclei by ruthenium during the lysis procedure was performed. The cell lysates from cells incubated with ruthenium complex were filtered through 0.2 μm nylon membrane (Whatman Centrex MF-5.0 filters), by centrifugation at 1,700–2,000 rpm. HeLa that were not incubated with ruthenium were detached with trypsin (no EDTA) and rinsed once with cold PBS. The cells were

resuspended in cold cell lysate (from the Ru-treated cells), vortexed, and incubated on ice for 9 min. The nuclei were pelleted by centrifugation at 2000 g (2,950 rpm) for 4 min at 4 °C, then washed twice with cold nuclei wash buffer. The nuclei were resuspended in cold nuclei wash buffer, vortexed, and triturated to break up clumps. The solution was filtered through a 35 μm cell strainer and stored on ice until analysis.

1.3: RESULTS AND DISCUSSION

1.3.1: STRATEGY TO MEASURE UPTAKE

The dipyridophenazine (dppz) complexes of ruthenium(II) act as reporters for non-aqueous environments, luminescing only when bound to the hydrophobic regions of membranes, nucleic acids, and other macromolecules.[26,27] Using their luminescence as a handle, we can readily analyze their cellular accumulation by confocal microscopy and flow cytometry.

Ru(II) polypyridyl complexes provide a systematic route for comparing factors affecting uptake, since ligands can be easily varied with respect to their characteristics and then metalated via the same synthetic strategy. In addition, the complexes under study are coordinatively saturated, with ligands that are inert to substitution. As a result, they are stable in buffer, medium, and the cellular environment. Their characteristic luminescence indicates that the complexes remain intact once inside the cell, as any decomposition or loss of ligands, albeit unlikely, would render the complexes non-luminescent.

A series of Ru(II) dppz complexes was synthesized for evaluation of their cellular uptake properties. Substituting the ancillary ligands on the dppz complex permits variation in the overall complex charge, size, and hydrophobicity (**Figure 1.1**).

1.3.2: CHARACTERISTICS OF THE RUTHENIUM COMPLEXES

Since the nature of the ancillary ligands can affect the luminescence properties of the ruthenium complexes, we measured their relative luminescence in CH_3CN and when bound to calf thymus DNA (**Table 1.1**). The complexes were excited at 488 nm, the same wavelength used for the confocal microscopy and flow cytometry experiments. The integrated emissions at 600–620 nm and 560–800 nm, the ranges recorded in flow cytometry and confocal microscopy analysis, respectively, are compared. All the complexes are non-luminescent in aqueous solution, but display luminescence in CH_3CN and in the presence of DNA. Also, there is no evidence of non-specific protein binding giving luminescence. Notably, $Ru(DIP)_2dppz^{2+}$ exhibits enhanced emission compared to the other complexes.

The lipophilicity of a compound can have a large influence on its cellular uptake. A common measure of a compound's lipophilicity is its octanol-water partition coefficient (*P*), defined as the ratio of the equilibrium concentrations of the dissolved compound in 1-octanol and water. This value is usually given in the form of its logarithm to base 10 (log *P*). Measurement of the partition coefficient can be performed by the "shake-flask" method or by HPLC analysis in comparison to reference substances.[28] We include the partition coefficients of our ruthenium complexes, obtained by the

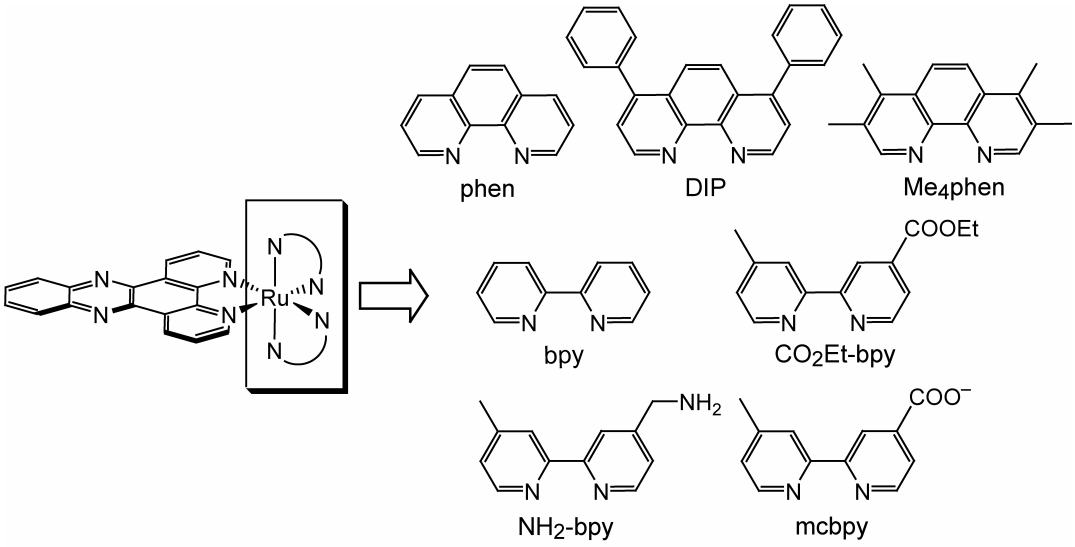

Figure 1.1: Dipyridophenazine complexes of Ru(II).

Table 1.1: Characteristics of the Ru complexes

ancillary ligand of RuL_2dppz	relative emission intensity in CH_3CN[a] 600–620 nm	relative emission intensity w/DNA[a,b] 600–620 nm	relative emission intensity in CH_3CN[a] 560–800 nm	relative emission intensity w/DNA[a,b] 560–800 nm	octanol/H_2O partition coefficient (log *P*)[c]	diameter (Å)[d]
bpy	1.0	1.0	1.0	1.0	-2.50	16.2
CO_2Et-bpy	1.8	1.1	2.2	1.4	-0.76	20.4
mcbpy	1.2	0.6	1.7	0.6	-0.43	18.2
NH_2-bpy	0.6	1.6	0.9	1.6	n.d.	17.8
phen	1.2	2.3	1.2	2.0	-1.48	16.2
Me_4phen	0.2	0.3	0.4	0.4	-0.79	17.4
DIP	2.7	2.7	2.6	2.4	1.30	20.4

[a]Excited at 488 nm; integrated emission over the indicated range. 10 μM Ru was used, except for $Ru(DIP)_2dppz^{2+}$ in Tris buffer, where a lower concentration was used due to poor solubility; emission values were scaled accordingly. [b]Luminescence values with DNA were obtained at saturation. [c]Cl^- salt. [d]Diameters were estimated using Titan. Data not determined are indicated by n.d.

shake-flask method, in **Table 1.1**. The only complex to prefer the octanol phase to water is $Ru(DIP)_2dppz^{2+}$.

Another factor that may affect a compound's uptake profile is its size. The diameters of our ruthenium complexes were estimated using the program Titan, and these are listed in **Table 1.1**. The largest complexes are $Ru(DIP)_2dppz^{2+}$ and $Ru(CO_2Et\text{-}bpy)_2dppz^{2+}$ at approximately 20.4 Å in diameter, and the smallest complexes are $Ru(phen)_2dppz^{2+}$ and $Ru(bpy)_2dppz^{2+}$ at 16.2 Å in diameter.

1.3.3: FLOW CYTOMETRY ANALYSIS OF UPTAKE

Flow cytometry allows the rapid quantification of luminescence intensity of individual cells as they pass single file through the laser beam, with thousands of cells analyzed in a few minutes. For our studies, we employed TO-PRO-3, a membrane impermeable dye, to stain dead cells and exclude them from analysis. The resulting data for the cell population can be displayed as a histogram of luminescence intensity versus number of cells. Uptake for different ruthenium complexes may be compared using the mean luminescence intensity of the cell population.

We used flow cytometry to examine the effect of ancillary ligand variation on the accumulation of dipyridophenazine complexes of Ru(II) in the human cervical cancer cell line, HeLa. Cells were incubated with 10 μM RuL_2dppz (where L = bpy, phen, NH_2-bpy, CO_2Et-bpy, mcbpy, Me_4phen, and DIP) for 2 h at 37 °C. The mean luminescence intensity of cells exposed to $Ru(DIP)_2dppz^{2+}$ ranges from 11-fold to 47-fold greater than that of the other complexes, and this difference is too large to be due solely to the

superior brightness of $Ru(DIP)_2dppz^{2+}$ (**Figure 1.2**, **Table 1.2**). The lipophilic DIP ligand seems to facilitate uptake, despite the larger size of the complex. Consistent with its intermediate lipophilicity, $Ru(Me_4phen)_2dppz^{2+}$ exhibits less efficient uptake than $Ru(DIP)_2dppz^{2+}$, but still better than the other complexes. $Ru(phen)_2dppz^{2+}$, $Ru(bpy)_2dppz^{2+}$, $Ru(NH_2\text{-}bpy)_2dppz^{4+}$, and $Ru(CO_2Et\text{-}bpy)_2dppz^{2+}$ are taken up to some extent, but little luminescence is evident for $Ru(mcbpy)_2dppz$. The lower emission intensity of $Ru(mcbpy)_2dppz$ with nucleic acids contributes to its relatively poor luminescence inside cells but cannot fully account for it. Likely, its reduced overall charge impairs its ability to use the membrane potential as a driving force for cellular entry (see Chapter 2). Accordingly, $Ru(NH_2\text{-}bpy)_2dppz^{4+}$, with its increased positive charge, exhibits slightly better uptake than $Ru(bpy)_2dppz^{2+}$.

These results are in agreement with uptake studies on cisplatin analogues, where the complexes with the greatest lipophilicity exhibit the highest uptake. Although, for the Pt complexes, all were hydrophilic, with octanol-water partition coefficients of < 1.[12]

1.3.4: CONFOCAL MICROSCOPY IMAGING

1.3.4.1: UPTAKE AND LOCALIZATION OF THE RU COMPLEXES

The subcellular distribution of our dipyridophenazine complexes of Ru(II) was studied using confocal microscopy. $Ru(DIP)_2dppz^{2+}$, which exhibits the greatest uptake by flow cytometry analysis, accumulates predominantly in the cytoplasm of HeLa cells. Luminescence is evident in the cell interior within 2 h when incubated at 5 μM (**Figure 1.3A**). Under similar conditions (10 μM, 2 h), $Ru(Me_4phen)_2dppz^{2+}$ is observed

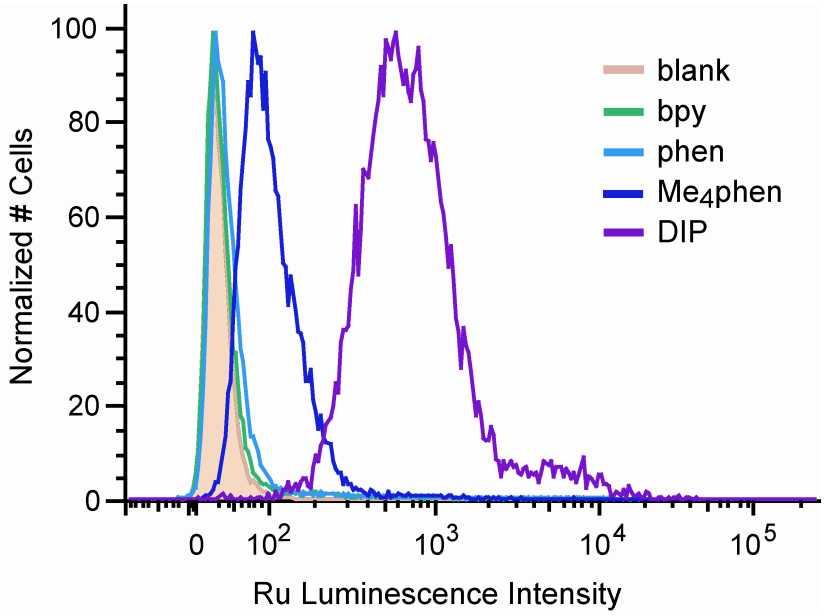

Figure 1.2: Flow cytometry analysis of ruthenium complex cellular uptake. HeLa cells were incubated with 10 μM RuL_2dppz^{2+} (where L = bpy, phen, Me_4phen, and DIP) for 2 h at 37 °C. Luminescence data were obtained by excitation at 488 nm with emission at 600–620 nm. Dead cells were excluded from analysis using the membrane impermeable dye TO-PRO-3.

Table 1.2: Cellular uptake of ruthenium complexes assayed by flow cytometry

ancillary ligand of RuL_2dppz	mean luminescence[a]
bpy	39 ± 2
NH_2-bpy	56 ± 4
CO_2Et-bpy	68 ± 4
mcbpy	25 ± 1
phen	79 ± 17
Me_4phen	107 ± 1
DIP	1169 ± 87

[a]HeLa cells were incubated with 10 μM ruthenium complex for 2 h at 37 °C. Ruthenium complexes were excited at 488 nm, with emission observed at 600–620 nm. The mean luminescence intensity of cells not treated with complex is 20. Each data point is the mean ± the standard deviation of three samples.

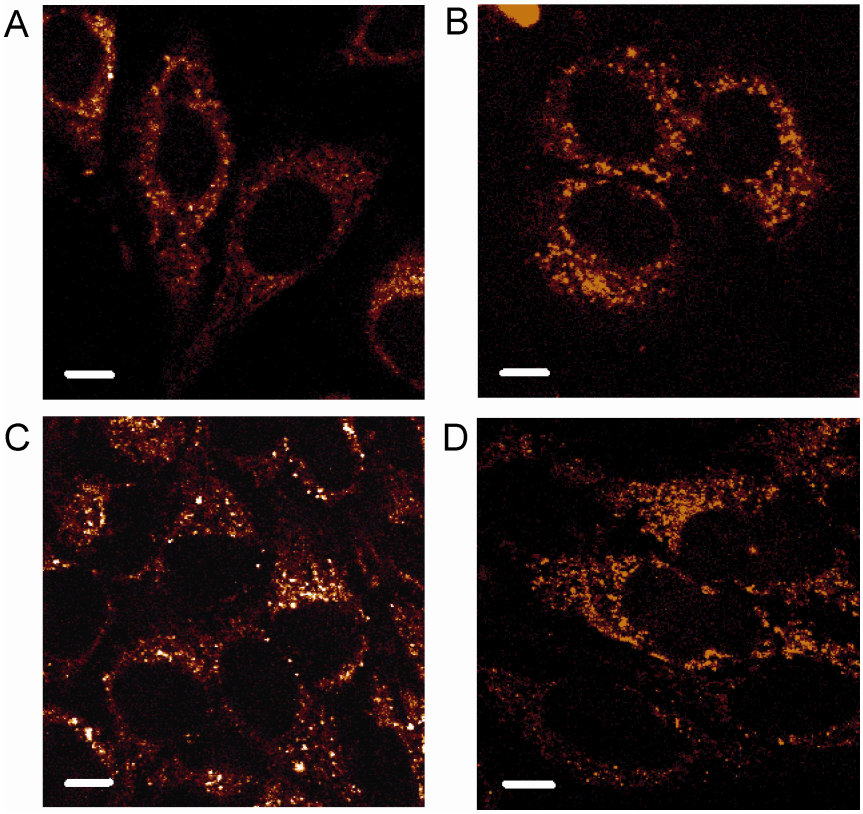

Figure 1.3: Confocal microscopy of HeLa cells incubated with dipyridophenazine complexes of Ru(II). (A) $Ru(DIP)_2dppz^{2+}$ (5 μM, 2 h).

(B) $Ru(Me_4phen)_2dppz^{2+}$ (10 μM, 2 h). (C) $Ru(phen)_2dppz^{2+}$ (20 μM, 24 h).

(D) $Ru(bpy)_2dppz^{2+}$(20 μM,72 h). Scale bars are 10 μm.

inside the cytoplasm of cells (**Figure 1.3B**). All of the other complexes, including $Ru(bpy)_2dppz^{2+}$ and $Ru(phen)_2dppz^{2+}$, which display limited uptake at 10 μM and 2 h by flow cytometry analysis, are also internalized, though longer incubation times and/or higher concentrations are required to obtain high-quality confocal images (**Figures 1.3C, 1.3D**). Inside the cell, the complexes are likely protected from water by macromolecular binding, without which quenching in the cytosol is expected.

At a slightly higher concentration and longer incubation time (10 μM, 12 h), there is a small increase in the amount of $Ru(DIP)_2dppz^{2+}$ in the nucleus, as shown by line plot quantitation (**Figure 1.4**), though the majority of complex remains in the cytoplasm. Longer incubations (5 μM, 72 h) do not produce a preference for the nucleus.

For most of the complexes, their exact location in the cytoplasm is difficult to discern. However, for $Ru(bpy)_2dppz^{2+}$, some of the luminescence has a stringy appearance that is characteristic of mitochondria (**Figure 1.5**). The putative mitochondrial staining is less intense than the additional, globular staining; as a result, it is visible in many but not all cells.

1.2.4.2: LIVE VERSUS FIXED CELL IMAGING

Cell fixation can sometimes alter the subcellular distribution of compounds. For example, some peptide-fluorophore conjugates have been shown to move from the cytoplasm to the nucleus following fixation with formaldehyde.[16] We evaluated the effect of different fixation methods on the localization of $Ru(DIP)_2dppz^{2+}$.

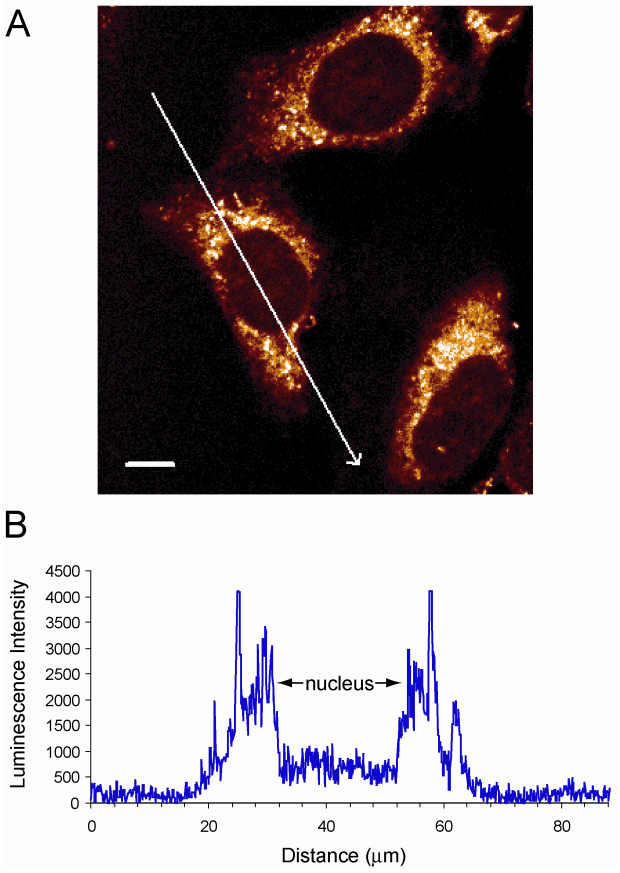

Figure 1.4: Quantitation of nuclear uptake. (A) HeLa cells were incubated for 12 h with 10 μM $Ru(DIP)_2dppz^{2+}$. Scale bar is 10 μm. The arrow indicates the section taken for the line plot in (B).

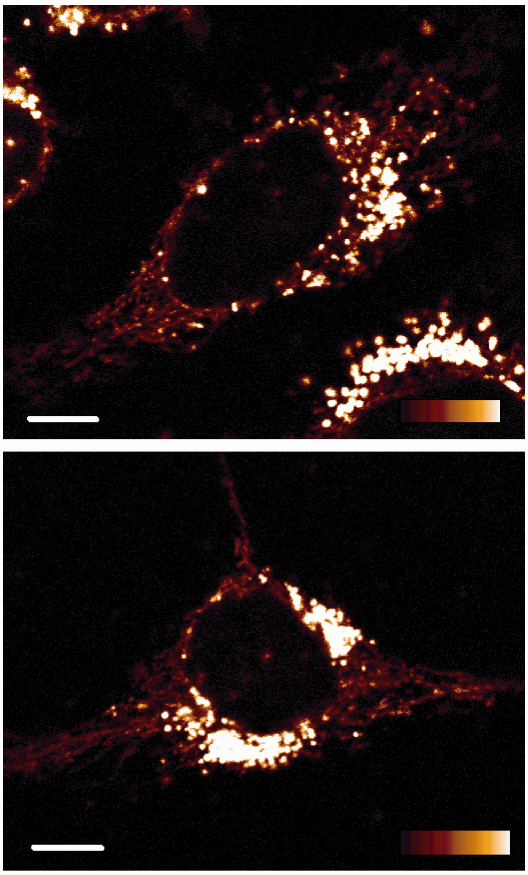

Figure 1.5: Subcellular localization of $Ru(bpy)_2dppz^{2+}$. HeLa cells were incubated with 40 μM $Ru(bpy)_2dppz^{2+}$ for 24 h. Scale bars (white) are 10 μm. The luminescence is shown on an intensity scale, denoted by the color-coded scale bars.

Live HeLa cells, incubated with 5 μM $Ru(DIP)_2dppz^{2+}$ for 2 h, were imaged before fixation to reveal cytoplasmic staining. Treatment with cold methanol causes a dramatic redistribution of the complex almost entirely to the nucleus (**Figure 1.6**). Though methanol enhances the luminescence of these complexes, the cells were rinsed with buffer following fixation and only trace methanol should remain. Likely, methanol solubilizes $Ru(DIP)_2dppz^{2+}$, aiding its diffusion into the now more permeable nucleus. Once inside the nucleus, the complex can bind to DNA, resulting in intense luminescence. In contrast, fixation with 2% formaldehyde does not produce any noticeable changes in the subcellular distribution of $Ru(DIP)_2dppz^{2+}$. Permeabilization of the formaldehyde-treated cells with 0.1% Triton X-100 (a non-ionic detergent), however, results in some nuclear accumulation of the complex. Rinsing with buffer following Triton X-100 treatment did not abrogate this effect, indicating that the increased luminescence is not conferred directly by presence of the fixative.

Formaldehyde appears to have fewer effects on ruthenium complex localization than methanol. Nevertheless, all of the confocal microscopy studies described elsewhere in this thesis were performed on live cells.

1.3.5: ANALYSIS OF ISOLATED NUCLEI

The metal complexes of the Barton lab target DNA, therefore we are keenly interested in the ability of our complexes to accumulate inside the nucleus. Hence, flow cytometry analysis of isolated nuclei was performed. In contrast to the live cell experiments, we cannot discriminate nuclei originating from dead cells versus those from

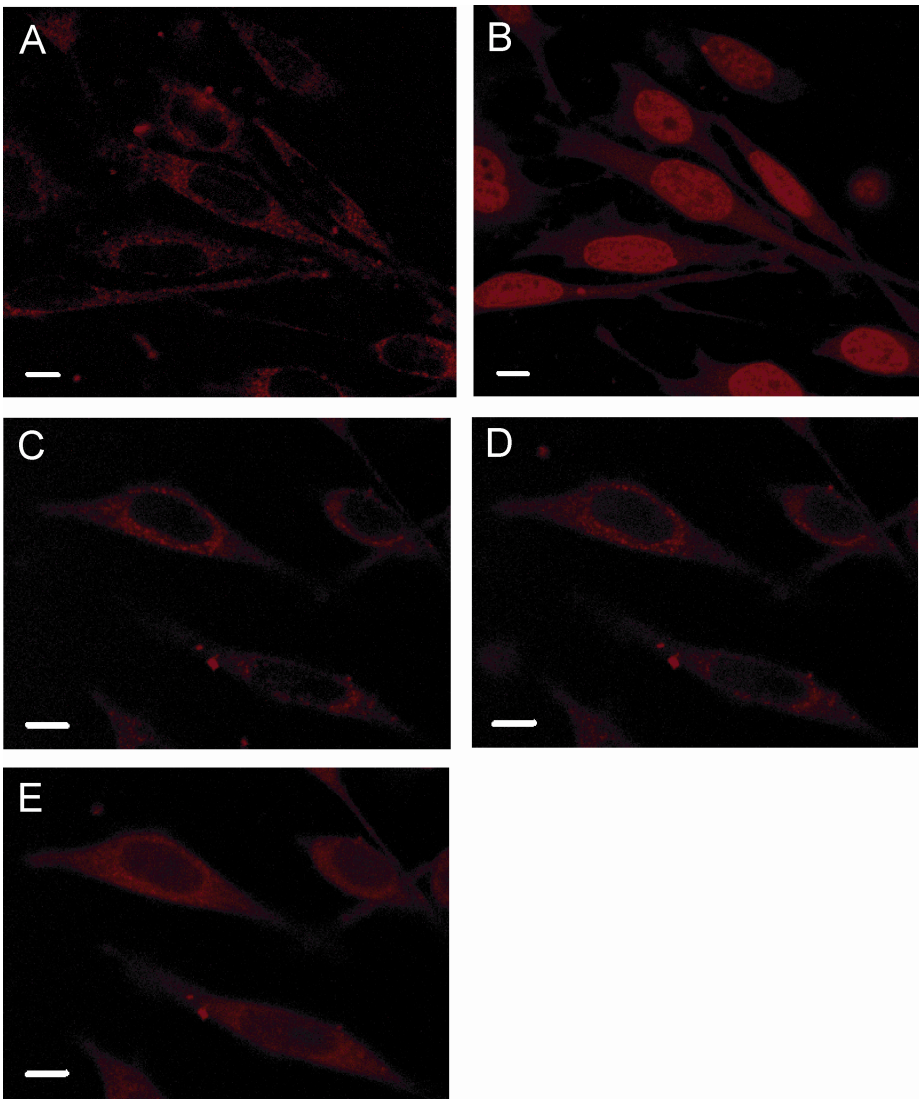

Figure 1.6: Effect of fixation on ruthenium complex subcellular localization. HeLa cells were incubated with 5 μM $Ru(DIP)_2dppz^{2+}$ for 2 h. Live cells (A, C) show cytoplasmic localization. After fixation of Ru-treated cells with methanol (B), the ruthenium complex relocates almost entirely to the nucleus. Fixation with 2% formaldehyde does not change the distribution (D), but treatment of the formaldehyde-fixed cells with 0.1% Triton X-100 increases the nuclear staining (E). Scale bars are 10 μm.

live cells. However, we expect that dead cells would accumulate a much greater amount of complex, resulting in nuclei that can be recognized by their increased staining. Also, analogous to the whole cell experiments, complex bound to the exterior of the nucleus cannot be distinguished from that in the interior. Therefore, confocal microscopy must be used to confirm internalization.

Nuclei isolated from HeLa cells incubated with 5 or 10 μM $Ru(DIP)_2dppz^{2+}$ for 2 h at 37 °C were analyzed for Ru uptake by flow cytometry. The mean luminescence intensity of the nuclei population increased substantially compared to nuclei from cells not treated with complex (**Figure 1.7**), consistent with nuclear uptake. Two populations of nuclei are seen in the histogram, with the population at very high luminescence likely coming from dead cells. Nuclei from cells incubated with 10 μM complex show greater luminescence than those incubated with 5 μM complex. There is also a positive correlation between length of incubation (2–24 h) and intensity of the ruthenium luminescence.

In order to isolate the nuclei, the cells are lysed. Since this procedure also permeabilizes the nuclear envelope, there is a possibility that during cell lysis, ruthenium complex located in the cytoplasm could move into the nucleus. Thus, we performed the following control for contamination of nuclei by ruthenium during the lysis procedure. Cells, which had not been incubated with ruthenium complex, were lysed using cell lysate from cells incubated with complex. These nuclei showed similar luminescence as the untreated, autofluorescence controls, which indicates that no substantial crossover of

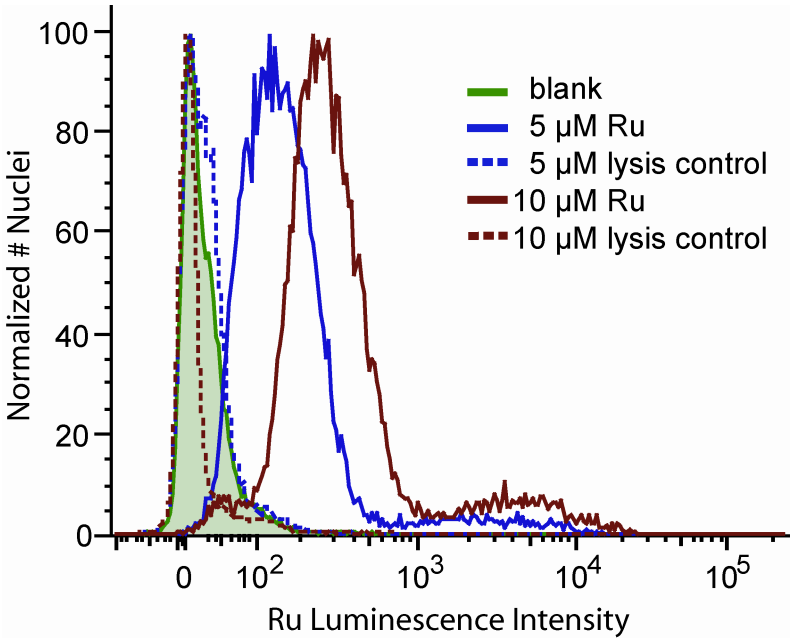

Figure 1.7: Flow cytometry analysis of nuclei isolated from HeLa cells incubated with 5 or 10 µM $Ru(DIP)_2dppz^{2+}$ for 2 h at 37 °C. Controls were performed to evaluate the extent of Ru contamination into the nucleus from the cytoplasm during lysis. For these controls, cells were lysed using cell lysate from cells incubated with $Ru(DIP)_2dppz^{2+}$.

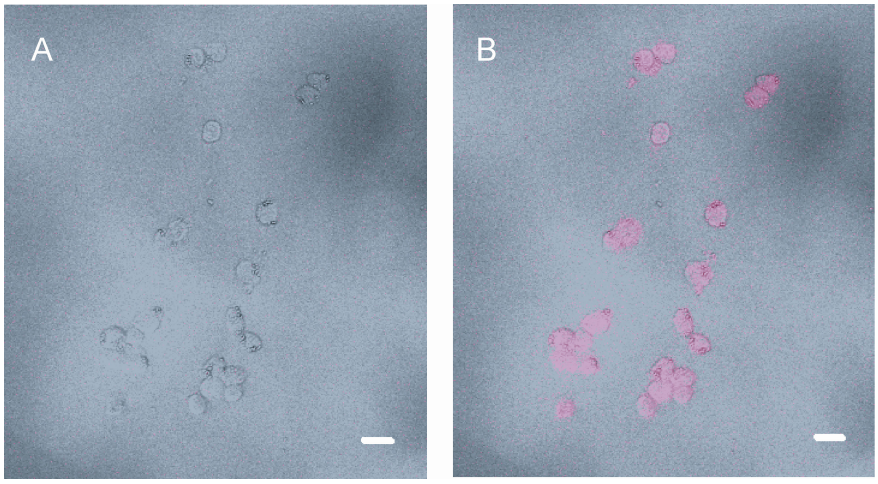

Figure 1.8: Confocal microscopy of nuclei isolated from HeLa cells incubated with 5 µM $Ru(DIP)_2dppz^{2+}$ for 2 h at 37 °C. (A) 1.1 µm optical slice. (B) 10.0 µm optical slice, which encompasses the entire thickness of the nuclei. Images are shown as overlay of the transmitted light image (gray) and the ruthenium luminescence (red). Scale bars are 20 µm.

ruthenium complex from the cytoplasm to the nucleus occurs during lysis.

Nuclei isolated from HeLa incubated with 5 μM $Ru(DIP)_2dppz^{2+}$ for 2 h at 37 °C were also examined by confocal microscopy (**Figure 1.8**). Ruthenium luminescence is not visible when the optical slice is set to 1.1 μm. When the optical slice is widened to 10.0 μm, thus increasing the sensitivity, the nuclei are brightly luminescent, which is consistent with the flow cytometry data. Ruthenium complex is associated with the nucleus, but the presence inside the nucleus cannot be established based on the 10.0 μm optical slice, because it encompasses the entire thickness of the nucleus.

Although we cannot confirm nuclear uptake using confocal microscopy of isolated nuclei when cells are treated with 5 μM $Ru(DIP)_2dppz^{2+}$, we can observe some complex inside the nucleus of intact cells when the incubation concentration is increased to 10 μM for 12 h (vide supra). Presumably, nuclei isolated from such cells would also show nuclear uptake. Furthermore, the increased luminescence of nuclei from treated versus untreated cells, the concentration dependence, and the time dependence observed by flow cytometry are all consistent with nuclear accumulation.

1.3.6: CELL LINE COMPARISON

The cellular accumulation and subcellular distribution of a compound can vary dramatically between cell types. For example, Dervan and co-workers have observed different degrees of nuclear uptake of pyrrole-imidazole polyamides depending on the cell line.[29] Hence, we compare the cellular uptake of our dipyridophenazine complexes of Ru(II) in human cancer cell lines derived from several different tissue types, namely

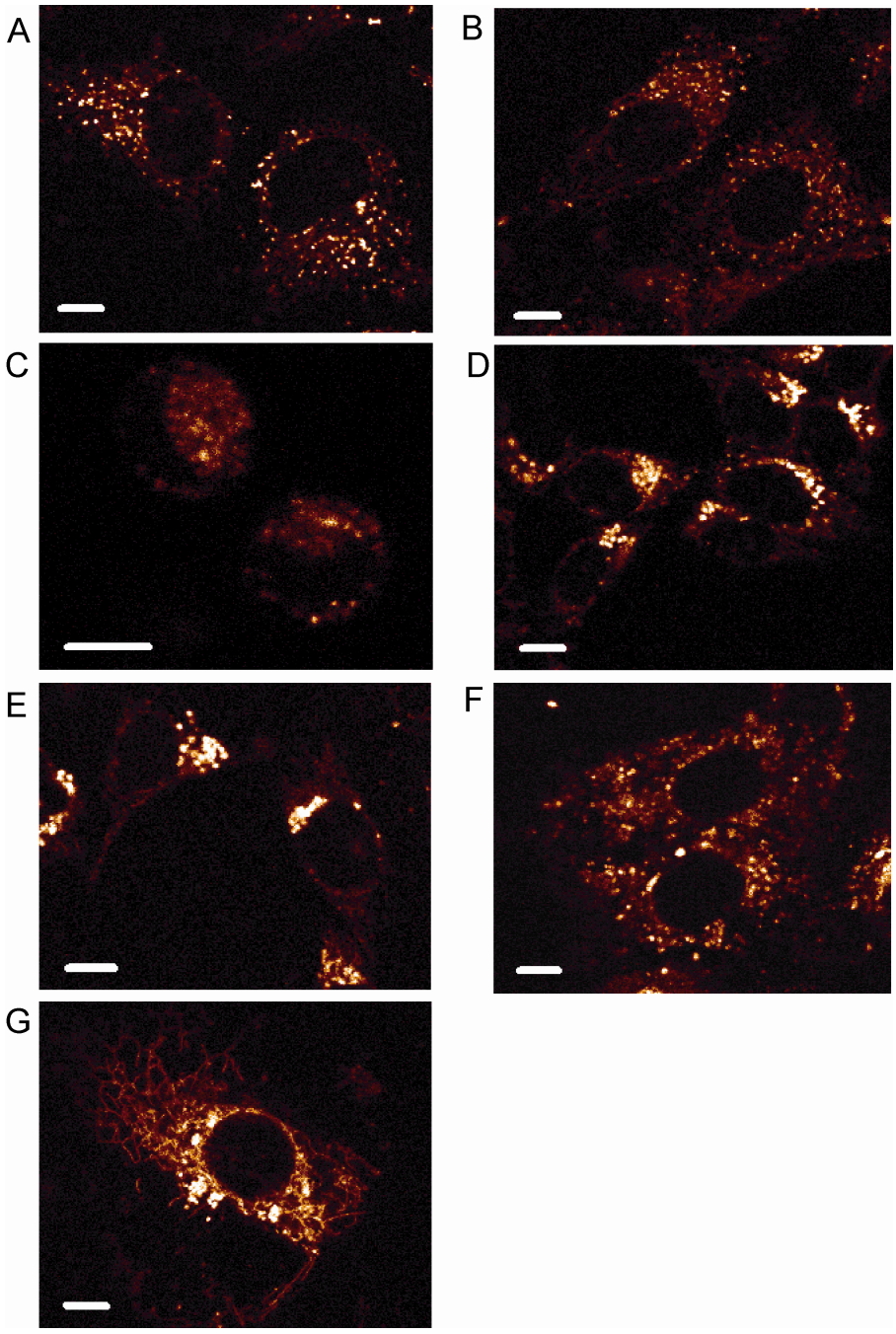

Figure 1.9: Accumulation of $Ru(bpy)_2dppz^{2+}$ by different cell lines. $Ru(bpy)_2dppz^{2+}$ (40 μM, 24 h) was incubated with (A) HeLa, (B) SKOV-3, (C) HT-29, (D) HCT116N, (E) HCT116O, (F) A-549, and (G) DU-145. Scale bars are 10 μm.

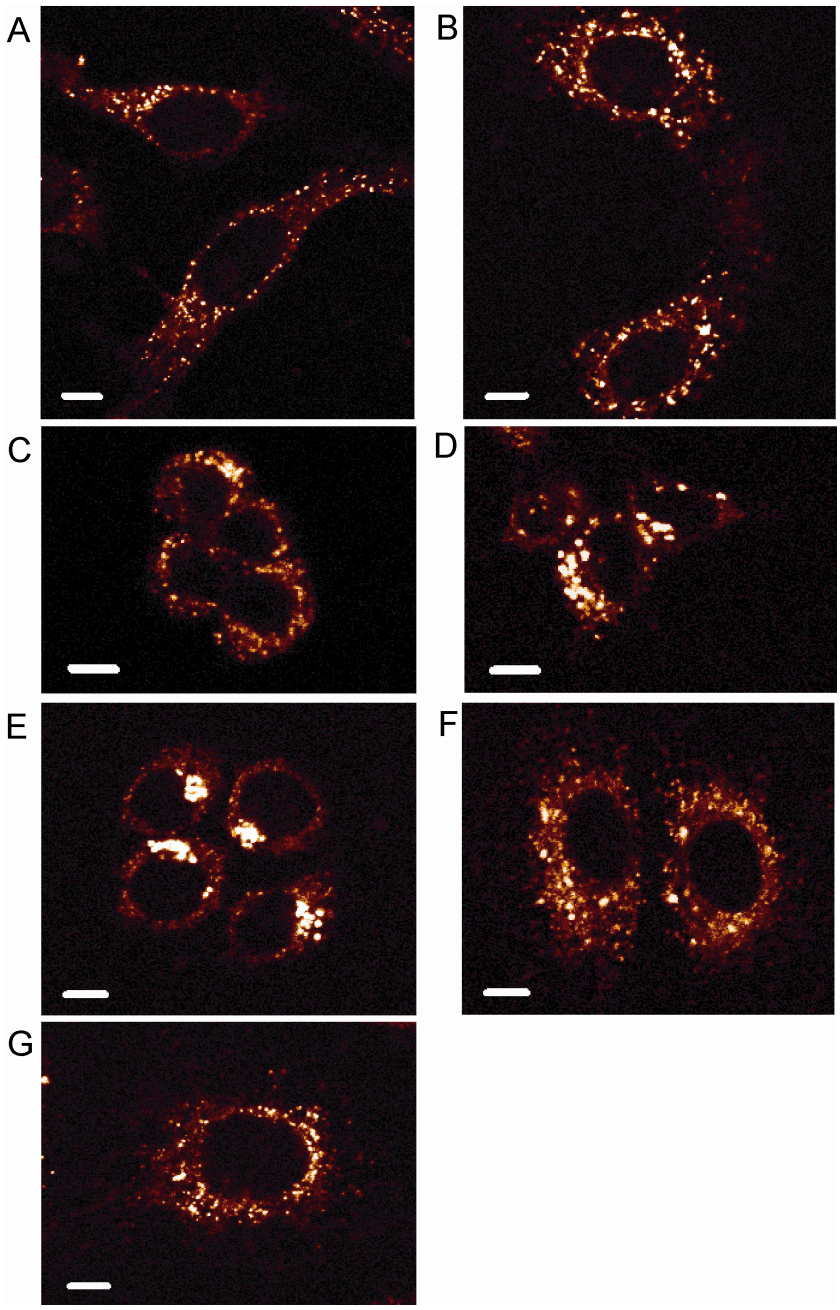

Figure 1.10: Accumulation of $Ru(phen)_2dppz^{2+}$ by different cell lines.

$Ru(phen)_2dppz^{2+}$ (40 μM, 24 h) was incubated with (A) HeLa, (B) SKOV-3, (C) HT-29, (D) HCT116N, (E) HCT116O, (F) A-549, and (G) DU-145. Scale bars are 10 μm.

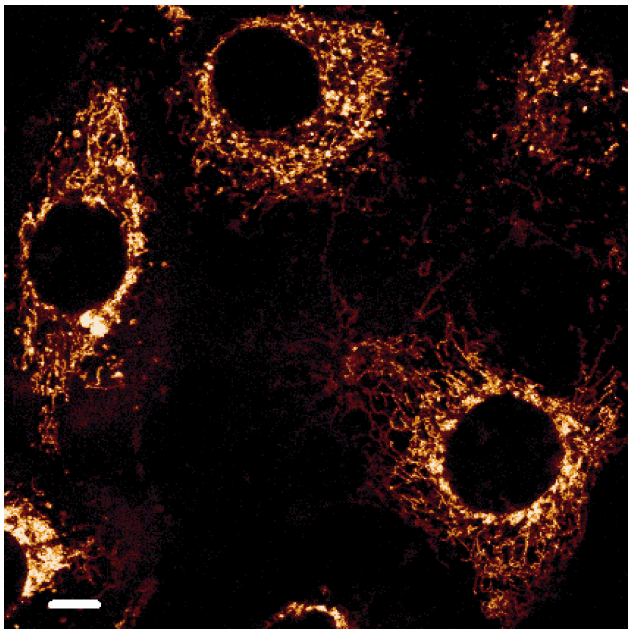

Figure 1.11: Accumulation of $Ru(bpy)_2dppz^{2+}$ in DU-145 cells. $Ru(bpy)_2dppz^{2+}$ was incubated at 40 μM for 24 h. The morphology of the staining is characteristic of mitochondria. Scale bar is 10 μm.

HeLa (cervix), SKOV-3 (ovary), HT-29 (colon), HCT116O (colon), HCT116N (colon), DU-145 (prostate), and A-549 (lung).

The cells, seeded at identical density, were incubated with 40 μM $Ru(bpy)_2dppz^{2+}$ or 40 μM $Ru(phen)_2dppz^{2+}$ in complete medium for 24 h then rinsed with buffer and imaged by confocal microscopy. Instrument settings were kept the same to allow for direct comparison of the luminescence intensity between the cell lines.

In all of the cell lines, both $Ru(bpy)_2dppz^{2+}$ and $Ru(phen)_2dppz^{2+}$ were localized in the cytoplasm but were absent from the nucleus (**Figures 1.9, 1.10**). The appearance of the cytoplasmic staining was similar between the lines, except for DU-145, where $Ru(bpy)_2dppz^{2+}$ seems to accumulate preferentially in mitochondria. Here, the staining displays a stringy shape that is characteristic of mitochondria (**Figures 1.9G, 1.11**). This pattern is also seen in HeLa treated with $Ru(bpy)_2dppz^{2+}$, but in a smaller percentage of the cells along with additional non-mitochondrial staining (**Figures 1.5, 1.9A**). Since the complex carries a positive charge, it may be pulled into the mitochondria in response to the membrane potential. However, the reason that mitochondrial localization is preferred by one cell line more than the others is not clear.

1.4: CONCLUSIONS

Using a series of dipyridophenazine complexes of Ru(II), we systematically compared the factors affecting cellular uptake and distribution. We find that $Ru(DIP)_2dppz^{2+}$ exhibits enhanced cellular accumulation compared to other complexes studied. Uptake appears to be facilitated by the lipophilic DIP ligand, even at the cost of

expanded size. Accordingly, $Ru(Me_4phen)_2dppz^{2+}$, which is intermediate in lipophilicity between $Ru(DIP)_2dppz^{2+}$ and $Ru(phen)_2dppz^{2+}$, enters cells with efficiency less than $Ru(DIP)_2dppz^{2+}$ but better than $Ru(phen)_2dppz^{2+}$. Reducing the charge of the complex hinders uptake: little luminescence is apparent for the neutral complex, $Ru(mcbpy)_2dppz$. In contrast, increasing charge from +2 to +4 results in a modest increase in uptake: luminescence of $Ru(NH_2\text{-}bpy)_2dppz^{4+}$ is slightly greater than that of $Ru(bpy)_2dppz^{2+}$. This correlation between charge and uptake is consistent with the plasma membrane potential serving as the driving force for cellular entry.

The complexes accumulate in the cytoplasm of live cells but are mostly excluded from the nucleus. However, flow cytometry analysis of nuclei isolated from cells treated with $Ru(DIP)_2dppz^{2+}$ are consistent with some nuclear entry, and nuclear staining is apparent by confocal microscopy when the incubation concentration is sufficiently high (10 μM, 12 h). Importantly, the rhodium analogues that we are exploring as potential therapeutic agents have been demonstrated to exert their biological effect in a manner dependent on direct binding to DNA,[6] implying that these complexes reach the nucleus. The present studies suggest that the population responsible for activity represents a fraction of the total compound inside the cell.

Ruthenium luminescence in the cytoplasm is uneven, which could indicate association with organelles, though the exact subcellular localization is not clear. This staining pattern is consistent across several different human cancer cell lines, with two exceptions. For HeLa and DU-145 cells incubated with $Ru(bpy)_2dppz^{2+}$, the morphology of the staining pattern is characteristic to that of mitochondria (**Figures 1.5, 1.11**).

Furthermore, we demonstrate that confocal microscopy and flow cytometry, in concert, are effective techniques for characterizing internalization and distribution of luminescent transition metal complexes. Ruthenium analogues in particular can be readily tested without special instrumentation or complicated synthesis; they can be excited by the 488-nm laser, common to most confocal microscopy and flow cytometry systems. Statistics on thousands of cells of varied cell type, under different incubation conditions, and using a range of metal complexes can be generated to provide a powerful complement in the design of metal complexes for biological application.

These data establish that the ruthenium complexes indeed accumulate in human cancer cell lines isolated from a variety of tissue types. In the following chapters, we will explore the mechanism of uptake and strategies to direct the compounds to the nucleus.

1.5: REFERENCES

1. Bruijnincx, P. C. A.; Sadler, P. J. *Curr. Opin. Chem. Biol.* **2008,** *12,* 197–206.
2. Jakupec, M. A.; Galanski, M.; Arion, V. B.; Hartinger, C. G.; Keppler, B. H. *Dalton Trans.* **2008,** 183–194.
3. Montgomery, C. P.; Murray, B. S.; New, E. J.; Pal, R.; Parker, D. *Acc. Chem. Res.* **2009,** *42,* 925–937.
4. Hart, J. R.; Glebov, O.; Ernst, R. J.; Kirsch, I. R.; Barton, J. K. *Proc. Natl. Acad. Sci. U. S. A.* **2006,** *103*, 15359–15363.
5. Zeglis, B. M; Pierre, V. C.; Barton, J. K. *Chem. Commun.* **2007**, 4565–4579.
6. Ernst, R. J.; Song, H.; Barton, J. K. *J. Am. Chem. Soc.* **2009,** *131,* 2359–2366.
7. Lipinski, C. A.; Lombardo, F.; Dominy, B. W.; Feeney, P. J. *Adv. Drug Delivery Rev.* **2001,** *46,* 3–26.
8. Hall, M. D.; Okabe, M.; Shen, D. W.; Liang, X. J.; Gottesman, M. M. *Annu. Rev. Pharmacol. Toxicol.* **2008,** *48,* 495–535.
9. New, E. J.; Parker, D. *Org. Biomol. Chem.* **2009,** *7,* 851–855.
10. Jiménez-Hernández, M. E.; Orellana, G.; Montero, F.; Portolés, M. T. *Photochem. Photobiol.*, **2000,** *72,* 28–34.
11. Egger, A. E.; Rappel, C.; Jakupec, M. A.; Hartinger, C. G.; Heffeter, P.; Keppler, B. K. *J. Anal. At. Spectrom.* **2009,** *24,* 51–61.
12. Ghezzi, A.; Aceto, M.; Cassino, C.; Gabano E.; Osella, D. *J. Inorg. Biochem.* **2004,** *98,* 73–78.

13. Kirin, S. I.; Ott, I.; Gust, R.; Mier, W.; Weyhermüller, T.; Metzler-Nolte, N. *Angew. Chem. Int. Ed.* **2008,** *47,* 955–959.

14. Jonas, S. K.; Riley, P. A. *Cell Biochem. Funct.* **1991,** *9,* 245–253.

15. Davies, D.; C. Hughes, C. Dead cell discrimination. In *In Living Color: Protocols in Flow Cytometry and Cell Sorting,* 1st ed.; Diamond, R. A., DeMaggio, S., Eds.; Springer: Berlin, 2000.

16. Richard, J. P.; Melikov, K.; Vives, E.; Ramos, C.; Verbeure, B.; Gait, M. J.; Chernomordik, L. V.; Lebleu, B. *J. Biol. Chem.* **2003,** *278,* 585–590.

17. Hällbrink, M.; Oehlke, J.; Papsdorf, G.; Bienert, M. *Biochim. Biophys. Acta* **2004,** *1667,* 222–228.

18. Dickeson, J. E.; Summers, L. A. *Aust. J. Chem.* **1970,** *23,* 1023–1027.

19. McCafferty, D. G.; Bishop, B. M.; Wall, C. G.; Hughes, S. G.; Mecklenberg, S. L.; Meyer, T. J.; Erickson, B. W. *Tetrahedron* **1995,** *51,* 1093–1106.

20. Berg, K. E.; Tran, A; Raymond, M. K.; Abrahamsson, M.; Wolny, J.; Redon, S.; Andersson, M.; Sun, L. C.; Styring, S.; Hammarström, L.; Toftlund, H.; Åkermark, B. *Eur. J. Inorg. Chem.* **2001,** 1019–1029.

21. Hamachi, I.; Tanaka, S.; Tsukiji, S.; Shinkai, S.; Oishi, S. *Inorg. Chem.* **1998,** *37,* 4380–4388.

22. Sullivan, B. P.; Salmon, D. J.; Meyer, T. J. *Inorg. Chem.* **1978,** *17*, 3334–3341.

23. Leasure, R. M.; Ou, W.; Moss, J. A.; Linton, R. W.; Meyer, T. J. *Chem. Mater.* **1996,** *8,* 264–273.

24. Chambron, J.-C.; Sauvage, J.-P. *Chem. Phys. Lett.* **1991,** *182,* 603–607.

25. Holmlin, R. E.; Stemp, E. D. A.; Barton, J. K. *Inorg. Chem.* **1998,** *37*, 29–34.

26. Friedman, A. E.; Chambron, J.-C.; Sauvage, J.-P.; Turro, N. J.; Barton, J. K. *J. Am. Chem. Soc.* **1990,** *112,* 4960–4962.

27. Jenkins, Y.; Friedman, A. E.; Turro, N. J.; Barton, J. K. *Biochemistry* **1992,** *31,* 10809–10816.

28. Sangster, J. Experimental Methods of Measurement. *Octanol-Water Partition Coefficients: Fundamentals and Physical Chemistry;* John Wiley & Sons: Chichester, U.K., 1997.

29. Edelson, B.; Best, T.; Olenyuk, B.; Nickols, N. Doss, R.; Foister, S.; Heckel, A.; Dervan, P. *Nucleic Acids Res.* **2004,** *32,* 2802–2818.

CHAPTER 2: MECHANISTIC STUDIES OF RUTHENIUM COMPLEX CELLULAR UPTAKE*

2.1: INTRODUCTION

Transition metal complexes have tremendous potential as diagnostic and therapeutic agents. They can be exploited for their modularity, reactivity, imaging capabilities, redox chemistry, and their precisely defined three-dimensional structure. An increasing number of biological applications have been explored.[1–3] Complexes that are currently in clinical use include the platinum anticancer drugs, radiodiagnostic agents containing ^{99m}Tc, and gadolinium(III) magnetic resonance imaging contrast agents.

In order to design new metal-based therapeutics more rationally, an understanding of the physiological processing of metal complexes is required. Though cellular uptake is critical to the success of a drug or probe, few mechanistic details are known regarding metal complex uptake. Different entry mechanisms may be preferred depending on the application, as the mode of entry affects cell-type specificity, the rate of internalization, and the fate of the compound once inside the cell. For example, entry by diffusion affords broad cell-type specificity, a great advantage in the use of fluorescent probes for live cell imaging. Conversely, medicinal chemists may seek to deliver drugs to target organs, taking advantage of tissue-specific transporters[4] or receptors.[5] For each mode of entry, there are also drawbacks. With protein-mediated transport, the degree of modification of

* Adapted from Puckett, C. A.; Barton, J. K. Mechanism of cellular uptake of a ruthenium polypyridyl complex. *Biochemistry* **2008,** *47,* 11711–11716.

the molecule is limited because transport relies on recognition. With endocytosis, molecules are often trapped in endosomes and face degradation by lysosomal enzymes.

Ruthenium(II) polypyridyl complexes are useful for studying cellular uptake due to their facile synthesis, stability in aqueous solution, and luminescence. Using confocal microscopy and flow cytometry, we have examined the uptake of a series of dipyridophenazine (dppz) complexes of ruthenium.[6] Despite its larger size, the lipophilic $Ru(DIP)_2dppz^{2+}$, illustrated in **Figure 2.1**, accumulates in cells more quickly than $Ru(bpy)_2dppz^{2+}$ (where bpy = 2,2′-bipyridine) and $Ru(phen)_2dppz^{2+}$ (where phen = 1,10-phenanthroline). $Ru(DIP)_2dppz^{2+}$ enters cells within an hour at micromolar concentrations, providing a reasonable time window for uptake experiments. Details of the cellular uptake mechanism of $Ru(DIP)_2dppz^{2+}$ can then be applied to understanding uptake characteristics of other structurally similar cationic metal complexes.

The biological activity of ruthenium complexes was first examined by Francis Dwyer in the 1950s, where a full family of tris(polypyridyl) complexes was shown to have bacteriostatic and anti-viral activities.[7] More recently, many ruthenium complexes have been tested for therapeutic potential,[8] and two ruthenium anticancer drugs (NAMI-A and KP1019) have reached clinical trials.[9,10] Cellular uptake of some ruthenium(III) complexes appears to be mediated by the iron transport protein transferrin. KP1019 (indazolium *trans*-[tetrachlorobis(1*H*-indazole)ruthenate(III)]) binds transferrin with displacement of a chloride ligand, and is transported into cells with transferrin by receptor-mediated endocytosis.[5] Ruthenium complexes lacking a labile ligand such as

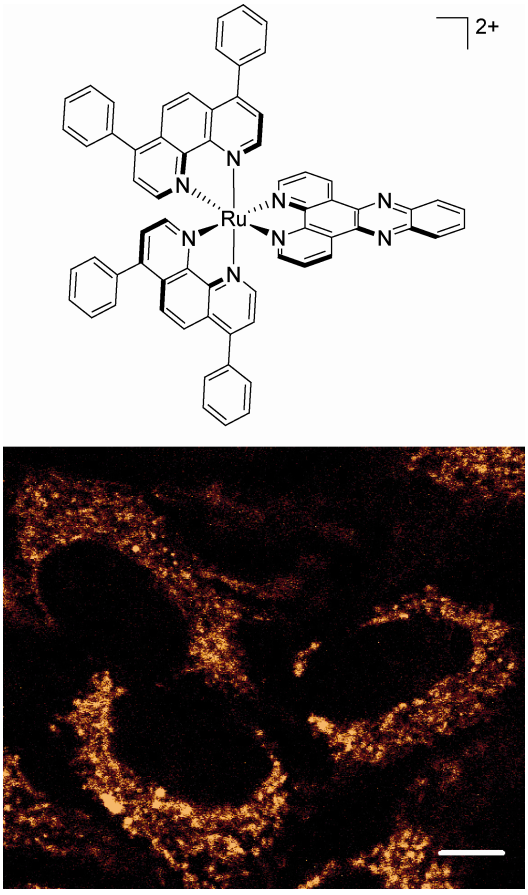

Figure 2.1: A luminescent ruthenium probe used to examine metal complex uptake. Top: Chemical structure of $Ru(DIP)_2dppz^{2+}$. Bottom: HeLa cells incubated with 5 μM $Ru(DIP)_2dppz^{2+}$ for 4 h, imaged by confocal microscopy. Note that the cytoplasm is extensively stained with the Ru complex. Scale bar is 10 μm.

chloride are unlikely to be able to enter cells in this manner and their mechanism of entry has not been established.

Such coordinatively saturated tris(chelate) ruthenium complexes furthermore serve as close fluorescent analogues of rhodium complexes that we have explored as potential chemotherapeutic agents.[11] These lipophilic, cationic rhodium complexes target single base mismatches in DNA and selectively inhibit cellular proliferation in mismatch repair-deficient cell lines.[3]

The main routes into a cell are endocytosis, active transport, facilitated diffusion, and passive diffusion. Due to its lipophilicity and positive charge, $Ru(DIP)_2dppz^{2+}$ likely traverses the membrane in response to the membrane potential, similar to other lipophilic cations such as tetraphenylphosphonium and rhodamine 123.[12,13] Here, we use chemical tools to elucidate the cellular uptake mechanism of $Ru(DIP)_2dppz^{2+}$, with the degree of uptake analyzed by flow cytometry.

2.2: EXPERIMENTAL PROTOCOLS

2.2.1.: MATERIALS

Cell culture reagents, transferrin-AlexaFluor488 conjugate, and TO-PRO®-3 were purchased from Invitrogen. Oligomycin, deoxyglucose, and the cation transporter inhibitors were obtained from Aldrich. Valinomycin was purchased from CalbioChem.

2.2.2: SYNTHESIS OF RU COMPLEXES

$Ru(DIP)_2dppz^{2+}$ and $Ru(phen)_2dppz^{2+}$ were synthesized as described previously (see also Chapter 1 of this text).[6] Briefly, $Ru(DIP)_2Cl_2$ and $Ru(phen)_2Cl_2$ were synthesized in an analogous fashion to $Ru(bpy)_2Cl_2$.[14] The dipyridophenazine (dppz) ligand was synthesized as previously described[15] and added to RuL_2Cl_2 by refluxing in ethanol-water for > 3 h to make $Ru(DIP)_2dppz^{2+}$ and $Ru(phen)_2dppz^{2+}$. The ethanol was removed by rotary evaporation, resulting in precipitation of $[Ru(DIP)_2dppz]Cl_2$, which was collected by filtration. $Ru(phen)_2dppz^{2+}$ was precipitated as the hexafluorophosphate salt, then returned to the chloride salt by Sephadex DEAE anion exchange column. The Ru complexes utilized are racemic mixtures of the two enantiomers.

2.2.3: CELL CULTURE

HeLa cells (ATCC, CCL-2) were maintained in minimal essential medium alpha with 10% fetal bovine serum, 100 units/mL penicillin, and 100 μg/mL streptomycin.

2.2.4: INDUCTIVELY COUPLED PLASMA MASS SPECTROMETRIC (ICP-MS) DETECTION OF RU

HeLa cells were grown to ~ 30% confluency in 75 cm^2 flasks and incubated with 5 μM $Ru(DIP)_2dppz^{2+}$ for 1 h at 37 °C in either medium with serum or medium without serum. The solution from the serum-free incubation was saved for circular dichroism measurements (described below). The cells were rinsed with PBS, detached with trypsin, and counted. The cells were isolated by centrifugation and digested in concentrated nitric

acid for 1.5 h at 60 °C. The solution was diluted with Millipore water to 2.0 mL for the incubation with serum and 20.0 mL for the serum-free incubation, adding nitric acid to give 2%. The Ru content was measured using a Hewlett Packard 4500 ICP-MS. Data are reported as the mean ± the standard deviation (n = 3).

2.2.5: ASSAY OF ENANTIOMERIC PREFERENCE IN RU UPTAKE

HeLa cells were grown to ~ 30% confluency in 75 cm^2 flasks and incubated with 5 μM $Ru(DIP)_2dppz^{2+}$ for 1 h at 37 °C in medium without serum and phenol red. After incubation, the medium was retrieved from the flask. The Ru complex was purified from the medium using a Waters C_{18} Sep-Pak. The solution was loaded onto a 1 g Sep-Pak equilibrated with water. The Sep-Pak was then rinsed with 150 mL water and 15 mL 20:80 $CH_3CN:H_2O$ with 0.1% TFA. The Ru complex was eluted with 90:10 $CH_3CN:H_2O$ with 0.1% TFA and lyophilized. For circular dichroism (CD) measurements, this isolated complex was dissolved in CH_3CN to give 8 μM complex. CD spectra were recorded on an AVIV 62 CD spectrometer.

2.2.6: METABOLIC INHIBITION

HeLa cells were detached from culture and treated with either 50 mM 2-deoxy-D-glucose and 5 μM oligomycin in PBS (to inhibit cellular metabolism) or 5 mM glucose in PBS for 1 h at 37 °C. Both solutions also contained 2.5 mg/mL bovine serum albumin fraction V (BSAV). The cells were then rinsed and suspended in either PBS with BSAV for the inhibition cells, or PBS with BSAV and 5 mM glucose for the control cells. The

cells were incubated with 10 mg/L transferrin-AlexaFluor488 or 5 μM $Ru(DIP)_2dppz^{2+}$ for 1 h at 37 °C. Following incubation, the transferrin-treated cells were rinsed with PBS and trypsinized to cleave the transferrin receptors from the cell surface.[16] The Ru-treated cells were rinsed. The cells were analyzed by flow cytometry. Ru-treated cells were not trypsinized following incubation, as rinsed cells and trypsinized cells gave the same mean luminescence in a control experiment: 282 ± 18 for the rinsed cells and 284 ± 23 for the trypsinized cells, following a 1 h incubation at 37 °C with 5 μM $Ru(DIP)_2dppz^{2+}$.

2.2.7: TEMPERATURE DEPENDENCE OF UPTAKE

HeLa cells were detached from culture and washed with Hanks' Balanced Salt Solution (HBSS) supplemented with 2.5 mg/mL BSAV. The cells were incubated with 5 μM $Ru(DIP)_2dppz^{2+}$ or $Ru(phen)_2dppz^{2+}$ for 2 h, or 10 mg/L transferrin-Alexa488 for 1 h, in HBSS with BSAV at 4 °C, ambient temperature (20–23 °C), or 37 °C. Transferrin-treated cells were trypsinized following incubation. The amount of uptake was analyzed by flow cytometry.

2.2.8: CATION TRANSPORTER INHIBITION

HeLa cells were detached from culture and washed with buffer (HBSS supplemented with BSAV), then pre-treated for 20 min with either 1 mM cation transporter inhibitor or buffer only. The cells were then incubated with 5 μM $Ru(DIP)_2dppz^{2+}$ for 1 h at ambient temperature. The cells were rinsed with buffer and Ru uptake was analyzed by flow cytometry.

2.2.9: MODULATION OF MEMBRANE POTENTIAL

HeLa cells were detached from culture and washed three times with either HBSS (containing 5.8 mM K^+) or high K^+-HBSS (containing 170 mM K^+), both supplemented with 2.5 mg/mL BSAV. Some of the cells in HBSS were pre-treated with 50 μM valinomycin for 30 min at 37 °C. The cells were incubated with 2 μM $Ru(DIP)_2dppz^{2+}$ for 1 h at 37 °C in one of the following solutions: HBSS, HBSS with valinomycin (to hyperpolarize the cells), or high K^+-HBSS (to depolarize the cells). The solutions also contained BSAV. After incubation, the cells were rinsed and the extent of uptake was analyzed by flow cytometry.

2.2.10: FLOW CYTOMETRY

Cells were detached from culture with EDTA (0.48 mM in PBS) and incubated at $1x10^6$ cells/mL with Ru complex (added from a concentrated DMSO stock) under conditions described above, then placed on ice. TO-PRO-3 was added at 1 μM immediately prior to flow cytometry analysis to stain dead cells. The fluorescence of ~ 20,000 cells was measured using a BD FACS Aria, exciting with the 488 nm laser for Ru and transferrin-AlexaFluor488, and with the 633 nm laser for TO-PRO-3. Emission was observed at 600–620 nm for Ru, 515–545 for AlexaFluor488, and 650–670 nm for TO-PRO-3. Cells exhibiting TO-PRO-3 fluorescence were excluded from the data analysis. Fluorescence data is reported as the mean ± the standard deviation (n = 3).

2.3: RESULTS

2.3.1: STRATEGY TO MEASURE UPTAKE

The dipyridophenazine (dppz) complexes of ruthenium serve as light switches for non-aqueous environments, luminescing only when bound to the hydrophobic regions of membranes, nucleic acids, and other macromolecules.[17,18] If the Ru complex decomposes or ligand substitution occurs, the resulting complex would no longer luminesce. Additionally the ligands themselves are not luminescent. Accordingly, the characteristic luminescence indicates that the complex inside the cell remains intact. We can use the luminescence of these ruthenium complexes to track their cellular uptake in both confocal microscopy and flow cytometry experiments. Confocal imaging confirms that $Ru(DIP)_2dppz^{2+}$ accumulates inside the cell rather than associating solely at the membrane surface, as seen in **Figure 2.1** and previously.[6] Ruthenium luminescence is observed throughout the cytoplasm, though mostly excluded from the nucleus. Flow cytometry, on the other hand, enables the rapid measurement of ruthenium luminescence intensity for multiple cell populations. Using primarily flow cytometry, we can then explore the cellular uptake mechanism of $Ru(DIP)_2dppz^{2+}$ by comparing the ruthenium luminescence following different incubation conditions.

2.3.2: ICP-MS MEASUREMENT OF RU UPTAKE

Inductively coupled plasma mass spectrometry (ICP-MS) measurements were performed to quantify the amount of Ru taken up by the cell. HeLa cells were treated with 5 μM $Ru(DIP)_2dppz^{2+}$ for 1 h at 37 °C in medium with or without serum. ICP-MS

measurements give 26.4 ± 6.3 amol of Ru per cell for the incubation in medium with serum, and 677 ± 73 amol per cell for the serum-free incubation. Assuming an average cell volume of 1.7 pL[19] and that the complex is evenly distributed throughout this volume, the Ru concentration in the cell is approximately 16 μM for incubation with serum and 398 μM for the serum-free incubation. These results indicate substantial concentration of the complex within the cell, with serum acting to attenuate the effective free ruthenium complex available in solution.

2.3.3: ENANTIOMERIC PREFERENCE IN UPTAKE

As racemic $Ru(DIP)_2dppz^{2+}$ was used for uptake experiments, we considered whether HeLa cells preferentially take in one enantiomer over the other. To test for enantioselectivity associated with uptake, we assayed for enantiomeric enrichment in the supernatant. Following incubation of 5 μM $Ru(DIP)_2dppz^{2+}$ with HeLa cells in serum-free medium, the Ru complex was recovered from the medium and the circular dichroism (CD) was examined. Serum-free medium was used for the incubation to remove any potential chiral bias created from interaction of the complex with serum proteins. ICP-MS determination of the Ru content of the cells confirms that a significant amount of Ru (~ 3% of the total) was taken in by the cells. Given this depletion, we estimate that an enantiomeric preference in uptake of 2.5:1 or greater would be detectable above instrument noise. However, the CD spectra of $Ru(DIP)_2dppz^{2+}$ after incubation with cells is within the level of the noise. This absence in optical activity indicates that any enantiomeric preference must be below this limit.

2.3.4: ENERGY-DEPENDENT UPTAKE MECHANISMS

Certain cellular uptake routes are energy-dependent, such as endocytosis[20] and active protein transport. These pathways are hindered when cells are incubated at low temperature (4 °C instead of 37 °C) or in ATP-depleted environments (e.g., from metabolic poisons). To determine whether $Ru(DIP)_2dppz^{2+}$ enters cells by an energy-dependent process, the complex was incubated with HeLa cells after ATP depletion by deoxyglucose (a glucose analogue that inhibits glycolysis) and oligomycin (an inhibitor of oxidative phosphorylation).[21, 22] As transferrin is internalized by clathrin-mediated endocytosis, fluorescently (AlexaFluor488) labeled transferrin was used as a positive control. The cellular uptake of $Ru(DIP)_2dppz^{2+}$ remains essentially unchanged when cells are under metabolic inhibition, with a mean luminescence of 659 ± 12 compared to 675 ± 10 for the cells not treated with deoxyglucose and oligomycin (**Figure 2.2**). Thus $Ru(DIP)_2dppz^{2+}$ appears to enter cells by an energy-independent process. In contrast, metabolic inhibition dramatically reduces the endocytosis of transferrin, demonstrated by the large decrease in the mean fluorescence from 3034 ± 52 to 210 ± 5.

The temperature dependence of $Ru(DIP)_2dppz^{2+}$ uptake was also explored. HeLa cells were incubated with the complex at 4 °C, ambient temperature (20–23 °C), and 37 °C (**Figure 2.3**). The mean Ru luminescence increases with incubation temperature, from 589 ± 17 at 4 °C to 826 ± 71 at 37 °C. Given the lipophilicity of $Ru(DIP)_2dppz^{2+}$, the increase in cellular uptake with temperature could also be the result of improved solubility in buffer at higher temperatures. To test this hypothesis, the temperature dependence of uptake was studied for a similar but more soluble complex,

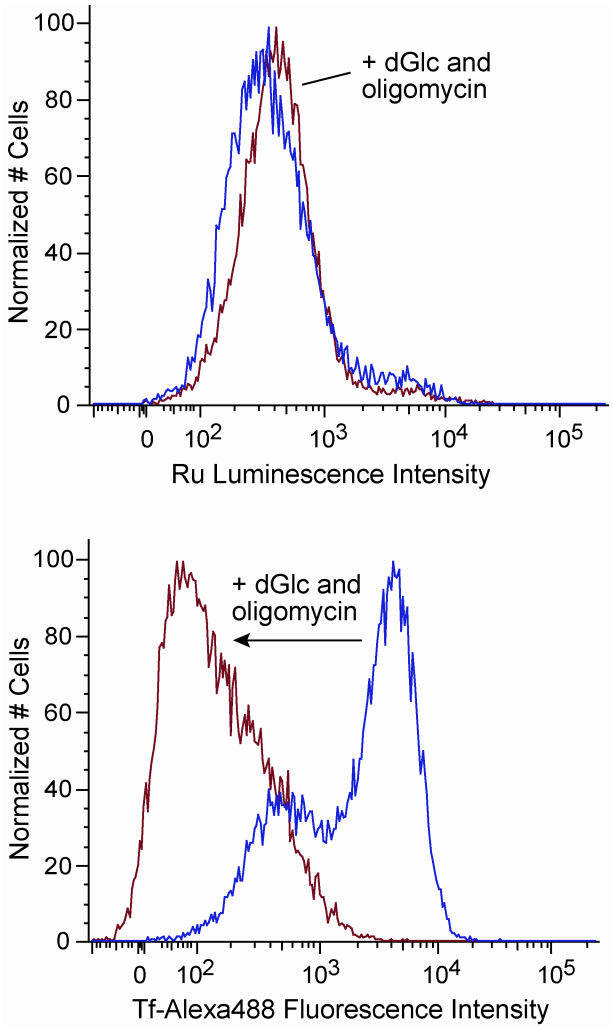

Figure 2.2: Flow cytometry measuring Ru incorporation used to examine the effect of metabolic inhibition on $Ru(DIP)_2dppz^{2+}$ cellular uptake. HeLa cells were pretreated for 1 h with 50 mM deoxyglucose (dGlc) and 5 μM oligomycin, then rinsed and incubated with 5 μM $Ru(DIP)_2dppz^{2+}$ or 10 mg/L transferrin-AlexaFluor488 (Tf-Alexa488) for 1 h. Cells treated with inhibitors (red) are compared to control cells (blue). Top: $Ru(DIP)_2dppz^{2+}$ uptake. Bottom: transferrin-AlexaFluor488 uptake.

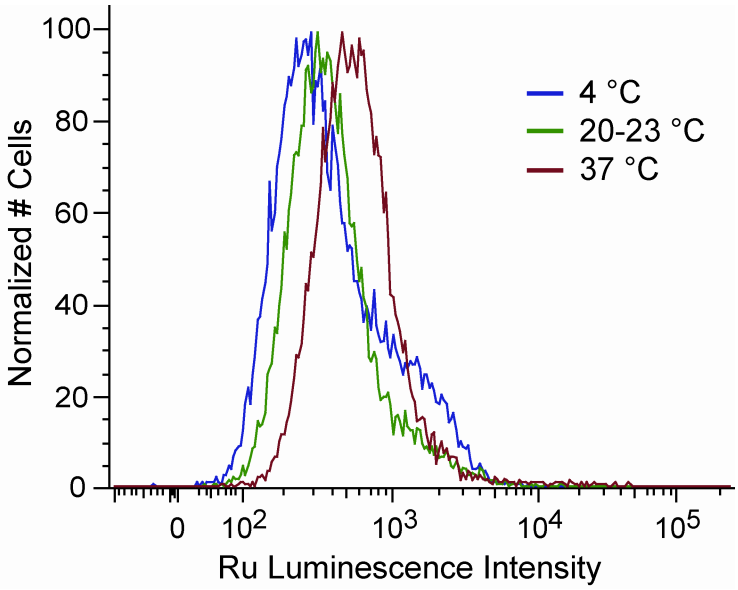

Figure 2.3: Effect of incubation temperature on $Ru(DIP)_2dppz^{2+}$ cellular uptake measured by flow cytometry. HeLa cells were incubated with 5 μM $Ru(DIP)_2dppz^{2+}$ for 2 h at 4 ºC, ambient temperature (20–23 ºC), or 37 ºC.

$Ru(phen)_2dppz^{2+}$. In this case, the mean luminescence remains roughly the same at the different incubation temperatures, 133 ± 10 at 4 °C and 141 ± 3 at 37 °C. Transferrin internalization was significantly more sensitive to temperature, with the mean fluorescence increasing from 480 ± 7 at 4 °C to 4071 ± 167 at 37 °C.

2.3.5: EFFECT OF ORGANIC CATION TRANSPORTER INHIBITORS

Organisms use polyspecific organic cation transporters (OCTs) for the distribution of endogenous organic cations and the absorption, distribution, and elimination of cationic drugs and toxins.[23] These transporters facilitate the diffusion of structurally diverse compounds. OCT substrates are typically organic cations and weak bases, though some neutral compounds and anions are also transported. Expression of the OCTs varies by tissue type. The carnitine and cation transporter OCTN2 has the most widespread tissue distribution among the OCTs, and its expression has been detected in some cancer cell lines, including HeLa.[24] Numerous compounds that inhibit OCT-mediated transport have been identified. Procainamide inhibits across the OCT family (including OCT1–3, OCTN1, and OCTN2). Tetraethylammonium ion is translocated by most of the OCTs, while other *n*-tetraalkylammonium salts inhibit OCT1 and OCT2, and for some OCTN1.[25]

To investigate whether $Ru(DIP)_2dppz^{2+}$ crosses the membrane using an organic cation transporter, uptake of $Ru(DIP)_2dppz^{2+}$ in the presence of OCT inhibitors was analyzed. HeLa cells were incubated with 1 mM inhibitor for 20 min before addition of $Ru(DIP)_2dppz^{2+}$ for 1 h. For OCTs, the IC_{50}s of the inhibitors used are generally less than

1 mM. Procainamide has an IC_{50} of < 3 mM and cimetidine <2 mM for OCTN2. As shown in **Figure 2.4**, the extent of uptake was analyzed by flow cytometry. Significantly, the *n*-tetraalkylammonium salts and procainamide do not appreciably alter the cellular uptake of $Ru(DIP)_2dppz^{2+}$. Within error, the cells have a similar mean luminescence intensity. The complex does not appear to use an organic cation transporter for entry into HeLa cells.

2.3.6: EFFECT OF MEMBRANE POTENTIAL

The plasma membranes of viable cells exhibit a membrane potential (−50 to −70 mV), with the inside of the cell negative with respect to the outside.[26] As $Ru(DIP)_2dppz^{2+}$ carries a positive charge, uptake may be driven by the potential difference across the cell membrane. The membrane potential in animal cells depends mainly on the K^+ concentration gradient. Here, the potential was reduced to close to zero by incubating the cells in buffer with potassium concentration equivalent to that found intracellularly (~170 mM).[27] This high potassium buffer (K^+-HBSS) was created by replacing sodium salts with equimolar potassium salts, while hyperpolarization of the membrane was achieved by adding valinomycin to low potassium buffer (HBSS).[28] Valinomycin is a cyclic peptide that selectively shuttles potassium ions across the membrane down the electrochemical potassium ion gradient, and it increases the membrane potential by exporting potassium from the cell.

$Ru(DIP)_2dppz^{2+}$ was incubated with HeLa cells for 1 h in either HBSS, HBSS with valinomycin (hyperpolarizes), or K^+-HBSS (depolarizes). The amount of Ru

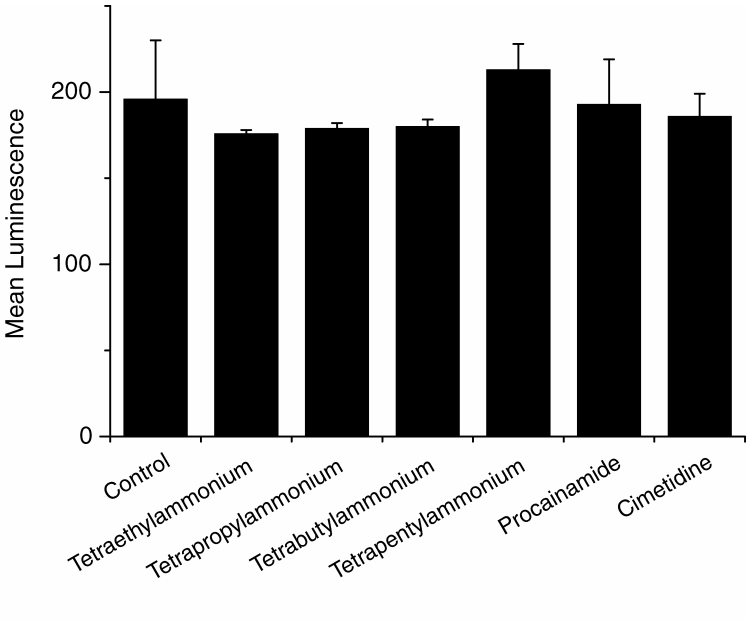

Figure 2.4: Effect of organic cation transporter inhibitors on $Ru(DIP)_2dppz^{2+}$ cellular uptake measured by flow cytometry. HeLa cells were pretreated with 1 mM inhibitor for 20 min, then 5 μM $Ru(DIP)_2dppz^{2+}$ was added for 1 h. Each data point is the mean ± the standard deviation of three samples.

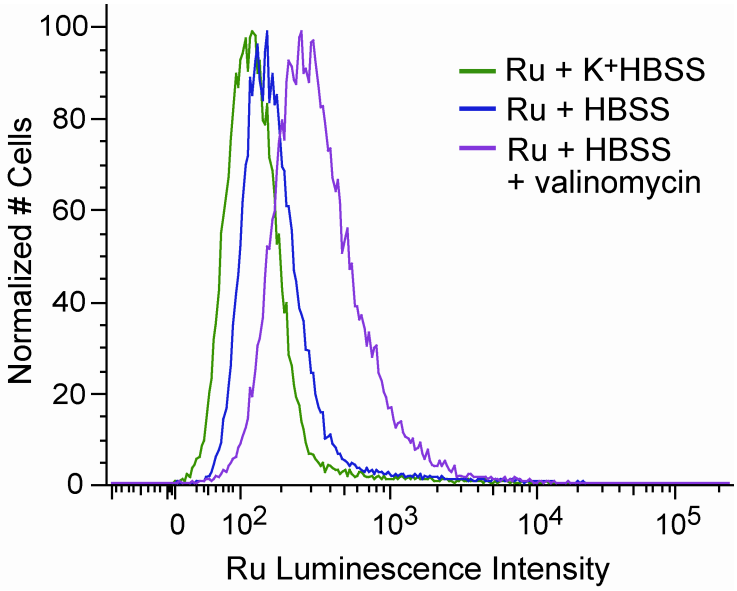

Figure 2.5: Effect of modulating the plasma membrane potential on $Ru(DIP)_2dppz^{2+}$ cellular uptake determined by flow cytometry. HeLa cells were incubated with 2 μM $Ru(DIP)_2dppz^{2+}$ in Hanks' Balanced Salt Solution (HBSS), HBSS with 50 μM valinomycin to hyperpolarize the cells, or modified HBSS with 170 mM potassium (K^+-HBSS) to depolarize the cells.

complex uptake was analyzed by flow cytometry (**Figure 2.5**). Depolarization of the plasma membrane reduces the uptake of $Ru(DIP)_2dppz^{2+}$, decreasing the mean luminescence of the cells from 232 ± 5 to 154 ± 1. Conversely, hyperpolarization of the membrane with valinomycin clearly promotes Ru complex uptake, increasing the mean luminescence to 428 ± 13. These results indicate that the positively charged complex is being driven inside the cells at least in part by the membrane potential.

2.4: DISCUSSION

Cellular uptake of small molecules can occur through energy-dependent (endocytosis, active transport) and energy-independent (facilitated diffusion, passive diffusion) processes. Metabolic inhibitors deplete the cell of energy, resulting in diminished uptake of molecules entering by endocytosis and active transport. HeLa cells treated with the metabolic inhibitors deoxyglucose and oligomycin show greatly reduced uptake (over 10-fold) of fluorescently labeled transferrin, which enters cells by endocytosis. On the other hand, deoxyglucose and oligomycin treatment cause no reduction of $Ru(DIP)_2dppz^{2+}$ cellular uptake, suggesting an energy-independent mode of entry. In fact, the midpoint of the luminescence intensity profile increases slightly in cells facing metabolic inhibition, though the mean fluorescence remains approximately the same. If $Ru(DIP)_2dppz^{2+}$ is actively exported, this efflux would be slowed under energy depletion and could explain the small increase. In contrast with the metabolic inhibition data, $Ru(DIP)_2dppz^{2+}$ uptake decreases slightly with lower temperature (4 °C versus 37 °C), consistent with energy-dependent transport. The difference is not as dramatic as

for transferrin, however, whose fluorescence changes 8-fold. Given that $Ru(DIP)_2dppz^{2+}$ is poorly soluble in buffer, this change may be due to improved solubility with temperature. Accordingly, a similar but more soluble complex, $Ru(phen)_2dppz^{2+}$, shows constant uptake at different temperatures. Low temperature also increases membrane viscosity, via decreased membrane fluidity, which can impair diffusion through the membrane.

The possible role of an organic cation transporter (OCT) in translocation of $Ru(DIP)_2dppz^{2+}$ across the membrane was also explored. These transporters facilitate the diffusion of endogenous organic cations as well as a variety of drugs and toxins. $Ru(DIP)_2dppz^{2+}$ uptake is not significantly altered in cells co-incubated with OCT inhibitors, indicating that the complex is likely not an OCT substrate. This result is consistent with the large size of $Ru(DIP)_2dppz^{2+}$ (~ 20 Å diameter) compared to known OCT substrates.

The cellular uptake of $Ru(DIP)_2dppz^{2+}$ is, however, influenced by the membrane potential. Consistent with diffusion of a positively charged molecule, uptake increases at higher potential and decreases at lower potential. That severe metabolic impairment does not discourage complex uptake is also consistent with diffusion. As both passage through a channel or passive carrier and diffusion directly through the lipid bilayer are energy-independent and respond to changes in the membrane potential, other factors must be considered to distinguish between these two mechanisms. The ability of $Ru(DIP)_2dppz^{2+}$ to enter the cell despite cation transporter inhibition, its larger size than typical

transporter substrates, and its relatively slow rate of cellular accumulation implicate passive diffusion as the mechanism of entry.

Passive diffusion is less cell-type specific, allows greater freedom for modification of the complex than transport via membrane proteins, and does not lead to entrapment in endosomes, as often occurs with endocytosis. As a result, this mechanism of passive diffusion may portend the broad applicability of metal complexes in different cell types for different intracellular functions. Certainly these results provide some basis for considering the biological activities that have already been identified for cationic transition metal complexes.[3,7] Significantly, knowledge of the mechanism of cellular uptake of this ruthenium(II) polypyridyl complex can now be applied to the design of structurally similar metal complexes for therapeutic and diagnostic use.

2.5: REFERENCES

1. Zhang, C. X.; Lippard, S. J. *Curr. Opin. Chem. Biol.* **2003***, 7,* 481–489.
2. Boerner, L. J. K.; Zaleski, J. M. *Curr. Opin. Chem. Biol.* **2005,** *9,* 135–144.
3 Hart, J. R.; Glebov, O.; Ernst, R. J.; Kirsch, I. R.; Barton, J. K. *Proc. Natl. Acad. Sci. U. S. A.* **2006,** *103*, 15359–15363.
4. Sai, Y.; Tsuji, A. *Drug Discovery Today* **2004,** *9,* 712–720.
5. Li, H.; Qian, Z. M. *Med. Res. Rev.* **2002,** *22,* 225–250.
6. Puckett, C. A.; Barton, J. K. *J. Am. Chem. Soc.* **2007***, 129*, 46–47.
7. Dwyer, F. P.; Gyarfas, E. C.; Rogers, W. P.; Koch, J. H. *Nature* **1952,** *170,* 190–191.
8. Clark, M. J. *Coord. Chem. Rev.* **2003,** *236,* 209–233.
9. Hartinger, C. G.; Zorbas-Seifried, S.; Jakupec, M. A.; Kynast, B.; Zorbas, H.; Keppler, B. K. *J. Inorg. Biochem.* **2006,** *100*, 891–904.
10. Bergamo, A.; Sava, G. *Dalton Trans.* **2007,** 1267–1272.
11. Zeglis, B. M; Pierre, V. C.; Barton, J. K. *Chem. Commun.* **2007,** 4565–4579.
12. Ross, M. F.; Kelso, G. F.; Blaikie, F. H.; James, A. M.; Cocheme, H. M.; Filipovska, A.; Da Ros, T.; Hurd, T. R.; Smith, R. A. J.; Murphy, M. P. *Biochemistry (Moscow)* **2005,** *70,* 222–230.
13. Davis, S.; Weiss, M. J.; Wong, J. R.; Lampidis, T. J.; Chen, L. B. *J. Biol. Chem.* **1985,** *260,* 13844–13850.
14. Sullivan, B. P.; Salmon, D. J.; Meyer, T. J. *Inorg. Chem.* **1978,** *17*, 3334–3341.
15. Dickeson, J. E.; Summers, L. A. *Aust. J. Chem.* **1970,** *23,* 1023–1027.

16. Bleil, J. D.; Bretscher, M. S. *EMBO J.* **1982,** *1,* 351–355.

17. Friedman, A. E.; Chambron, J.-C.; Sauvage, J.-P.; Turro, N. J.; Barton, J. K. *J. Am. Chem. Soc.* **1990,** *112,* 4960–4962.

18. Jenkins, Y.; Friedman, A. E.; Turro, N. J.; Barton, J. K. *Biochemistry* **1992,** *31,* 10809–10816.

19. Wheatley, D. N.; Inglis, M. S.; Foster, M. A.; Rimington, J. E. *J. Cell Sci.* **1987,** *88,* 13–23.

20. Schmid, S. L.; Carter, L. L. *J. Cell Biol.* **1990,** *111,* 2307–2318.

21. Barban, S.; Schulze, H. *J. Biol. Chem.* **1961**, *236,* 1887–1890.

22. Slater, E. C. *Methods Enzymol.* **1967**, *10,* 48–57.

23. Koepsell, H. *Trends Pharmacol. Sci.* **2004,** *25,* 375–381.

24. Wu, X.; Prasad, P. D.; Leibach, F. H.; Ganapathy, V. *Biochem. Biophys. Res. Commun.* **1998**, *246,* 589–595.

25. Koepsell, H.; Lips, K.; Volk, C. *Pharmacol. Res.* **2007**, *24,* 1227–1251.

26. Lodish, H.; Berk, A; Zipursky, S. L.; Matsudaira, P.; Baltimore, D.; Darnell, J. E. *Molecular Cell Biology,* 4th ed.; Tenney, S., Ed.; W. H. Freeman and Co.: New York, 2000.

27. Ehrenberg, B.; Montana, V.; Wei, M.-D.; Wuskell, J. P.; Loew, L. M. *Biophys. J.* **1988,** *53,* 785–794.

28. Shapiro, H. M. *Methods* **2000,** *21,* 271–279.

CHAPTER 3: DIRECTING THE SUBCELLULAR LOCALIZATION OF A RUTHENIUM COMPLEX WITH OCTAARGININE[‡]

3.1: INTRODUCTION

In addition to crossing the cellular membrane, molecular probes and therapeutics must reach their intended location inside the cell. The 5,6-chrysenequinone diimine (chrysi) complexes of rhodium(III) that we are developing as potential chemotherapeutic agents target single base mismatches of DNA.[1–3] Therefore, we are interested in promoting their nuclear accumulation, which should increase their potency and reduce off-target effects.

Confocal microscopy studies on dipyridophenazine (dppz) complexes of Ru(II), luminescent analogues of our rhodium complexes, reveal that they accumulate in the cytoplasm but are predominantly excluded from the nucleus (see Chapter 1).[4] One may surmise, then, that only a fraction of the rhodium(III) chrysi complexes inside the cell are localizing in the nucleus.

A widely used strategy to improve both cellular uptake and nuclear localization is conjugation to a peptide. Cell-penetrating peptides (CPPs), such as the HIV Tat peptide and oligoarginine, facilitate the cellular uptake of many cargos, including peptides, proteins, oligonucleotides, plasmids, and peptide nucleic acids.[5–7] Some CPPs also act as nuclear localization signals (NLSs). Such peptides are rich in positively charged residues such as arginine or lysine and promote active transport through the nuclear pore

[‡] Adapted from Puckett, C. A.; Barton, J. K. Fluorescein redirects a ruthenium-octaarginine conjugate to the nucleus. *J. Am. Chem. Soc.* **2009,** *131,* 8738–8739.

complex.[8] However, the use of peptides is not a fail-proof method for nuclear localization, as entrapment in endosomes can occur, leaving the peptides unable to access the nuclear import machinery.

In earlier work, we prepared a chrysi complex of Rh(III) covalently tethered to D-octaarginine (D-R8) fluorescein and found that it rapidly localizes to the nucleus of HeLa cells.[9] As the rhodium complex itself is not fluorescent, fluorescein was attached to monitor the subcellular distribution of this Rh-D-R8 conjugate. However, the potential effects of the fluorescein on the cellular uptake properties cannot be ignored. Some laboratories have varied the fluorescent dye used to assess uptake of a cell-penetrating peptide and found some fluorophore-dependent changes.[10–12] Similarly, the uptake characteristics of pyrrole-imidazole polyamides have been shown to vary with the nature of the appended fluorophore.[13,14]

Luminescent ruthenium(II) polypyridyl complexes allow us to directly observe their subcellular localization, without need of a fluorescent tag. Furthermore, using these complexes, we can isolate the effect of a covalently attached fluorophore on the cellular uptake properties of the metal-peptide conjugate.

3.2: Experimental protocols

3.2.1: Materials and instrumentation

Media, cell culture supplements, Hanks' Balanced Salt Solution, and TO-PRO®-3 iodide were purchased from Invitrogen (Carlsbad, CA).

ESI mass spectrometry was performed at either the Caltech mass spectrometry facility or in the Beckman Institute Protein/Peptide Micro Analytical Laboratory. MALDI measurements were performed on an Applied Biosystems Voyager 6215. Absorption spectra were recorded on a Varian Cary 100 or Beckman DU 7400 spectrophotometer. HPLC was performed on an HP1100 system equipped with a diode array detector using a Vydac C_{18} reversed-phase semipreparative column.

3.2.2: SYNTHESIS OF RU-PEPTIDE CONJUGATES

Peptides, protected and resin-bound, were purchased from Anaspec (Fremont, CA); arginine was protected as its 2,2,4,6,7-pentamethyldihydrobenzofuran-5-sulfonyl (Pbf) derivative and lysine as its methyltrityl (Mtt) derivative. $Ru(phen)(bpy')(dppz)^{2+}$ was coupled to the peptide in an analogous manner to that previously described (where phen = 1,10-phenanthroline, bpy′ = 4-(3-carboxypropyl)-4′-methyl-2,2′-bipyridine, and dppz = dipyrido[3,2-*a*:2′,3′-*c*]phenazine).[9,15] Briefly, the acid of the ruthenium complex was coupled to the free N-terminal amine of the peptide by HOBT/HBTU or HATU activated coupling reaction. Fluorescein was added by reaction of fluorescein-5-isothiocyanate (5-FITC) with a lysine residue at the C-terminus. The peptides were cleaved from the resin using 95% trifluoroacetic acid, 2.5% triisopropylsilane, and 2.5% water for 3 h at ambient temperature and then precipitated by addition of cold diethyl ether. Conjugates were purified by reversed-phase HPLC using a water (0.1% trifluoroacetic acid)/acetonitrile gradient and characterized by MALDI-TOF or ESI mass spectrometry; Ru-octaarginine (Ru-D-R8): 2069.3 *m/z* (M^+) obsd, 2069.4 *m/z* (M^+) calcd,

Ru-octaarginine-fluorescein (Ru-D-R8-fluor): 2585.9 *m/z* (M^+) obsd, 2586.9 *m/z* (M^+) calcd, Ru-fluorescein (Ru-fluor): 668.7 *m/z* (M^{2+}) obsd., 668.7 *m/z* (M^{2+}) calcd. All conjugates employed in this study were used as their trifluoroacetate salts. Concentrations were determined by the absorption of $Ru(phen)(bpy')(dppz)^{2+}$; for Ru-D-R8-fluor and Ru-fluor, 361 nm, which is not obscured by fluorescein, was used (ε_{440}= 19,000 M^{-1} cm^{-1}; ε_{361}= 19,469 M^{-1} cm^{-1}).

3.2.3: CELL CULTURE

HeLa cells (ATCC, CCL-2) were maintained in minimal essential medium alpha with 10% fetal bovine serum (FBS), 100 units/mL penicillin, and 100 μg/mL streptomycin.

3.2.4: CONFOCAL MICROSCOPY

HeLa were seeded using 4000 cells in wells of a glass-bottom 96-well plate (Whatman, Inc.) and allowed to attach overnight. The complexes were incubated with HeLa cells in complete medium (medium with 10% fetal bovine serum) at 37 °C under the following conditions: Ru-D-R8 at 2–20 μM for 30 min, Ru-D-R8-fluor at 2–5 μM for 30 min, and Ru-fluor at 5 μM for 30 min and 20 μM for 41 h. The samples were then rinsed with Hanks' Balanced Salt Solution (HBSS) and imaged without fixation. Imaging was performed using a 63x/1.4 oil immersion objective on a Zeiss LSM 510 or a Zeiss LSM 5 Exciter inverted microscope. The optical slice was set to 1.1 μm. Ru-D-R8 was excited at 488 nm, with emission observed at 560+ nm. For Ru-D-R8-fluor and Ru-fluor,

the emission was collected as the combined emission of Ru and fluorescein (505+ nm), both of which are excited at 488 nm. For spectral confocal imaging, HeLa cells were incubated with 10 μM Ru-D-R8-fluor for 60 min at 37 °C, rinsed with HBSS, and analyzed. Emission was collected as a series of bands (10.7 nm width) from 500–720 nm using the multi-channel (META) detector.

3.3: RESULTS AND DISCUSSION

3.3.1: SYNTHESIS OF THE CONJUGATES

Three Ru(II) dipyridophenazine conjugates were synthesized: Ru-octaarginine (Ru-D-R8), Ru-octaarginine-fluorescein (Ru-D-R8-fluor), and Ru-fluorescein (Ru-fluor) (**Figure 3.1**). D-Arginine was chosen for its improved biostability over the L-enantiomer. The conjugates were prepared by solid-phase coupling of $Ru(phen)(bpy')(dppz)^{2+}$ to the N-terminal amine of the peptide. Addition of fluorescein to the C-terminus of the peptide was accomplished via a Mtt-protected lysine, which was selectively deprotected to yield the free ε-amine and reacted with fluorescein-5-isothiocyanate (**Figure 3.2**). For Ru-fluor, a single lysine residue, on solid support, was coupled to the ruthenium complex, followed by addition of fluorescein. Cleavage from the resin can be performed using standard Fmoc cleavage protocols, since the ruthenium complexes are found to be stable under these conditions.[15]

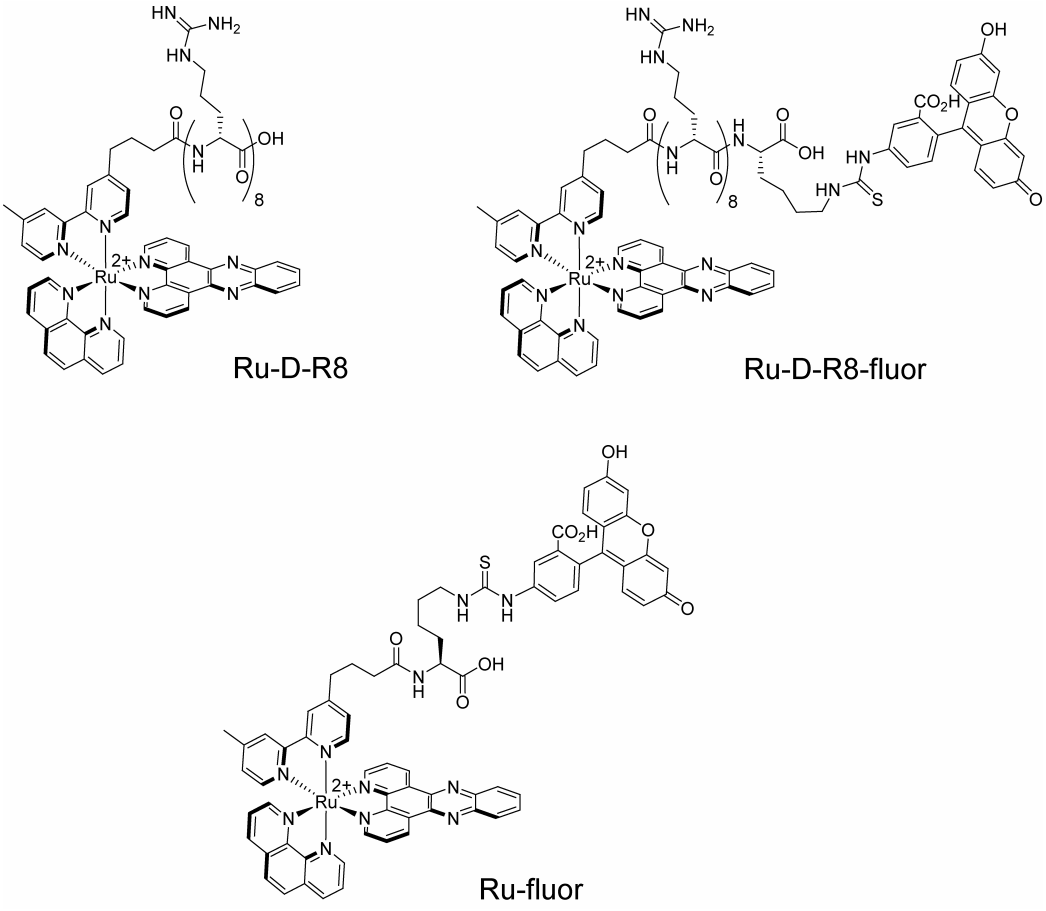

Figure 3.1: Chemical structures of the ruthenium conjugates.

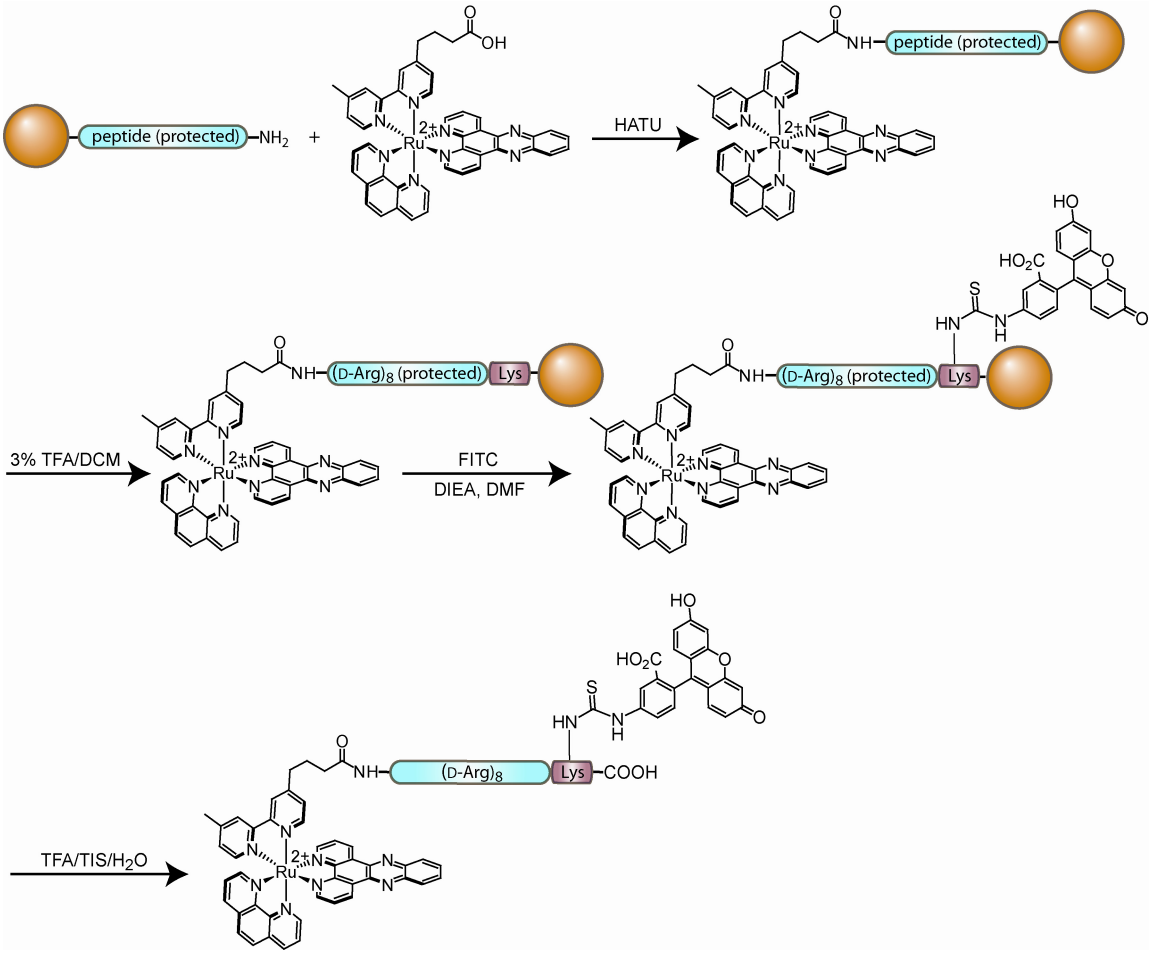

Figure 3.2: Synthesis of Ru-D-R8-fluor. Ru-fluor was synthesized in an analogous procedure using (Fmoc)Lys(Mtt) on the solid support instead of the peptide.

3.3.2: SUBCELLULAR LOCALIZATION OF RU-OCTAARGININE

HeLa cells incubated with Ru-D-R8 at 5 μM for 30 min exhibit punctate luminescence in the cytoplasm, with complete exclusion from the nucleus (**Figure 3.3**). The punctate distribution implicates endocytosis, a proposed internalization mechanism for oligoarginine CPPs, as its route into the cell.[16] Entrapment in endosomes would explain the lack of nuclear entry. In this context, the peptide changes the mode of uptake relative to unconjugated complexes, such as $Ru(phen)(bpy')(dppz)^{2+}$, $Ru(phen)_2dppz^{2+}$, and $Ru(bpy)_2dppz^{2+}$, which enter by passive diffusion.[17] As expected, for the peptide conjugates, cellular uptake is strongly enhanced compared to these unconjugated complexes; higher luminescence is evident in cell samples even after short incubation times. Notably, increasing the incubation time from 30 min to 2 h or 24 h does not change the subcellular localization of 5 μM Ru-D-R8 (**Figure 3.3**).

At higher concentrations, the distribution of Ru-D-R8 changes significantly. Up to 10 μM, the complex is restricted to punctate structures in the cytoplasm. At 15–20 μM, the cell population is heterogeneous. Some cells have only punctate cytoplasmic staining, while others exhibit additional diffuse cytoplasmic as well as nuclear and nucleolar staining (**Figure 3.4**). Nucleolar labeling is typical of D-octaarginine, as seen here, although not of L-octaarginine.[18] The fraction of cells in the latter population increases with concentration (**Table 3.1**). The nucleolar and punctate staining are of similar intensity, with fainter nuclear and cytoplasmic staining.

Population heterogeneity has been described for nonaarginine-fluorescein (R9-fluor).[19,20] What differentiates cells that have greater uptake and nuclear staining versus

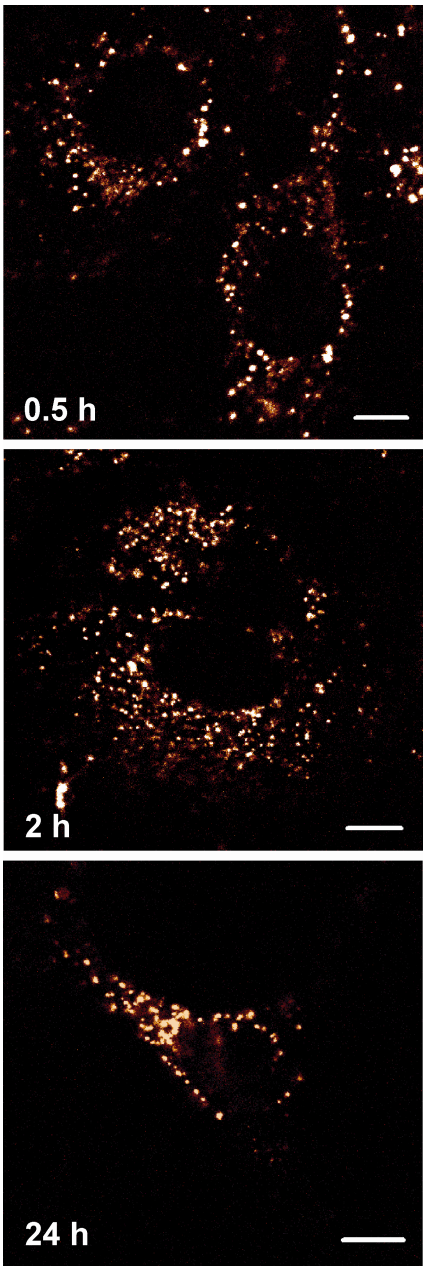

Figure 3.3: Cellular distribution of Ru-D-R8 following different durations of incubation. HeLa cells were incubated with 5 μM Ru-D-R8 in complete medium for 0.5 h, 2 h, or 24 h. The complex is localized in the cytoplasm at all three time points. Scale bars are 10 μm.

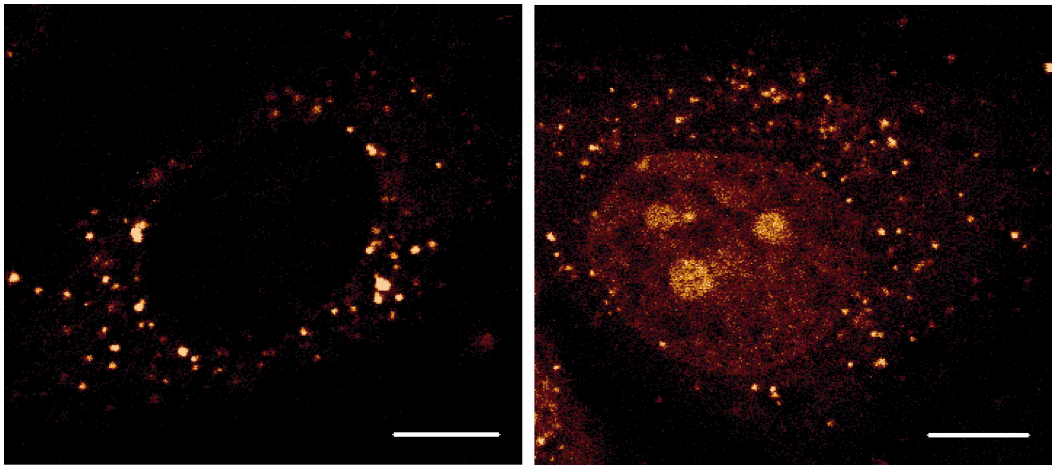

Figure 3.4: Cellular distribution of Ru-D-R8 at higher concentration. HeLa cells were incubated with 20 μM Ru-D-R8 for 30 min at 37 °C in complete medium. The cells shown exclude the membrane-impermeable dead cell dye TO-PRO-3. Some cells have only punctate staining of the cytoplasm (left) while others show additional staining of the nucleus and nucleoli as well as diffuse cytoplasmic staining (right). Scale bars are 10 μm.

Table 3.1: Percentage of HeLa cells with nuclear staining by Ru-octaarginine conjugates[a]

	Ru conjugate	
concn (μM)	Ru-D-R8	Ru-D-R8-fluor
2	0%	0%
5	0%	91%
10	0%	n.d.
15	38%	n.d.
20	60%	n.d.

[a]HeLa cells were incubated with Ru conjugate for 30 min at 37 °C in complete medium, then rinsed with HBSS and analyzed by confocal microscopy. ~50–100 cells were counted for each sample. Dead cells were excluded by their morphology. Data not determined are indicated by n.d.

those that have less is not clear, but these groups of cells do not represent distinct, stable phenotypes. Rothbard and coworkers sorted by flow cytometry the top and bottom 5% of stained cells, re-exposed them to R9-fluor, and re-analyzed them. These cells displayed a similarly broad range of uptake.[19]

A concentration threshold for diffuse cytoplasmic and nuclear labeling is a feature of oligoarginine-fluorophore conjugates and has been reported previously.[18,20,21] Above the extracellular threshold concentration, the peptides are postulated to enter by a non-endocytic mechanism in addition to the endocytic mechanisms evident at lower concentrations.

3.3.3: Effect of fluorescein on Ru-octaarginine localization

Remarkably, the Ru-octaarginine conjugate containing an appended fluorescein (Ru-D-R8-fluor) enters the nucleus under the same incubation conditions for which the complex without fluorescein is excluded. Ru-D-R8-fluor shows diffuse cytoplasmic and nuclear fluorescence, strong nucleolar staining, and some punctate cytoplasmic staining when incubated at 5 μM for 30 min with HeLa (**Figure 3.5**, center). Some cells have numerous fluorescent punctate structures, while others have relatively few. The intensity of fluorescence in the nucleoli is roughly equal to that of these punctate, vesicular structures. Notably, at this concentration, D-R8-fluor and the Rh(III) conjugate of D-R8-fluor also localize to the nucleus.[9] The threshold for Ru-D-R8-fluor nuclear entry is between 2 and 5 μM, significantly lower than that for Ru-D-R8 (**Table 3.1**).

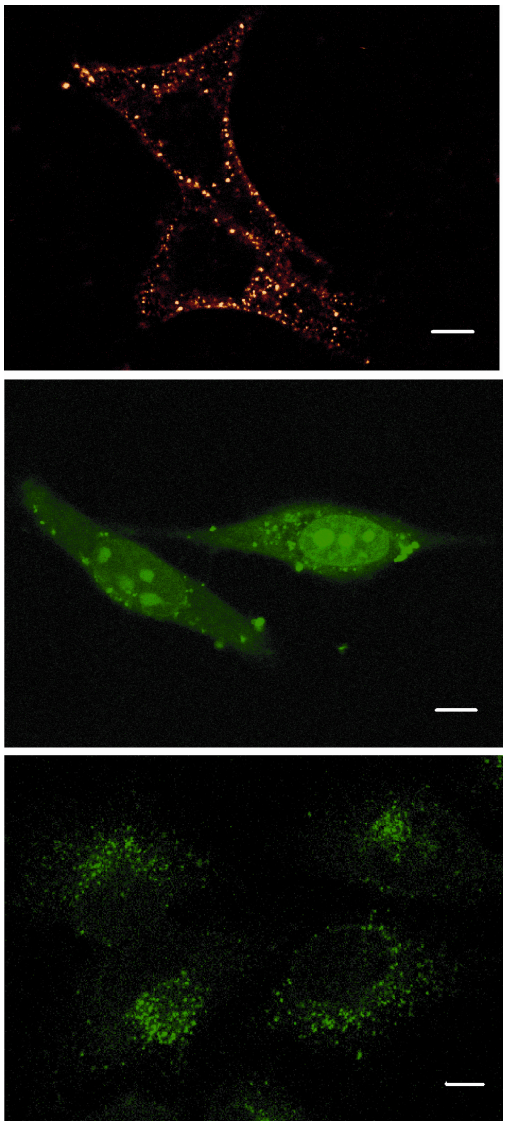

Figure 3.5: Cellular distribution of Ru conjugates. HeLa cells were incubated with 5 μM Ru-D-R8 for 30 min (top), 5 μM Ru-D-R8-fluor for 30 min (center), or 20 μM Ru-fluor for 41 h (bottom) at 37 °C in complete medium. Note that Ru-D-R8 is isolated to the cytoplasm while Ru-D-R8-fluor stains the cytosol, nucleus, and nucleoli. Ru-fluor shows only weak cytoplasmic staining. Scale bars are 10 μm.

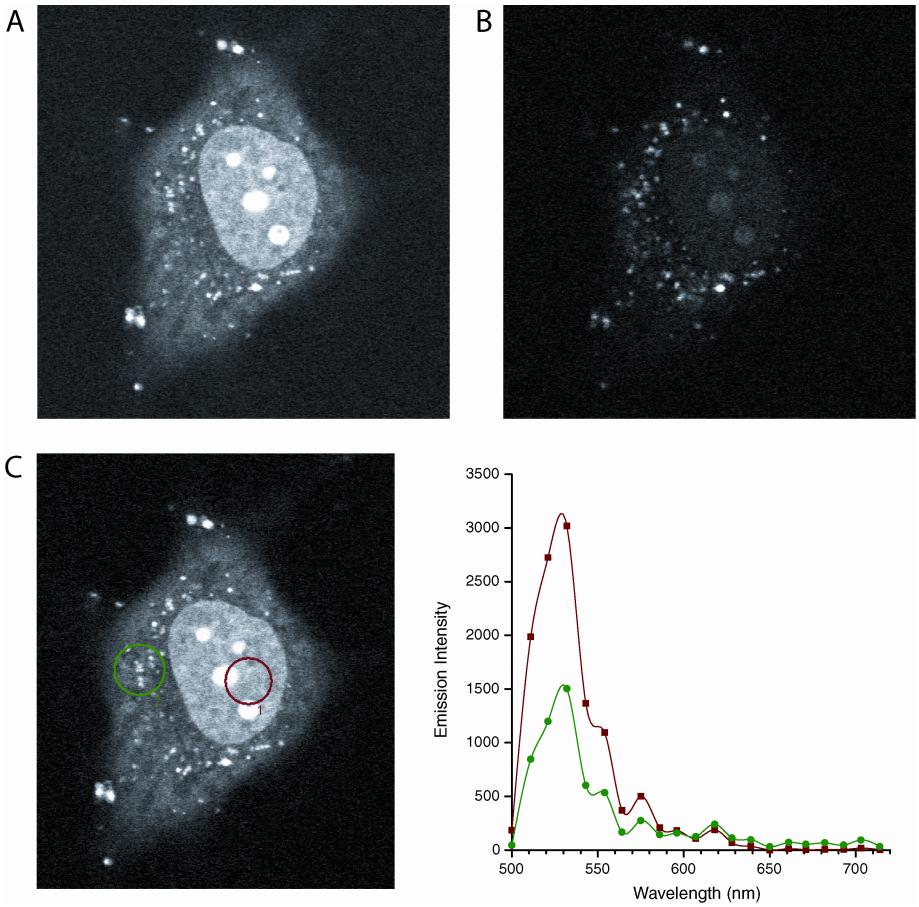

Figure 3.6: Spectral confocal imaging (10.7 nm bandwidth) of HeLa cells incubated with 10 µM Ru-D-R8-fluor for 60 min. (A) Emission at 521 nm. (B) Emission at 618 nm. (C) Emission spectra from nuclear (red) and cytoplasmic (green) regions. Fluorescein (521 nm) and ruthenium (618 nm) emission from the nucleus are apparent.

Not surprisingly, the Ru-fluorescein conjugate lacking octaarginine is unable to enter the cell under the same incubation conditions for which its octaarginine counterparts can translocate (5 μM for 30 min). The complex is poorly internalized even following a longer incubation time with higher concentration (20 μM for 41 h) (**Figure 3.5,** bottom). Given its significantly lower positive charge (as both the fluorescein and the internal carboxylic acid are likely partially deprotonated), the complex cannot as effectively use the membrane potential as a driving force for cellular entry.

Spectral confocal imaging of HeLa cells incubated with Ru-D-R8-fluor (10 μM, 60 min) was performed. Emission from both fluorescein (λ_{max} = 521 nm) and Ru (λ_{max} = 618 nm) are observed in the cytoplasm and in the nucleus, which indicates that the conjugate remains intact inside the cell (**Figure 3.6**).

What role is fluorescein playing in the uptake? Fluorescein, due to its greater lipophilicity versus the Ru moiety, increases the interaction of Ru-D-R8-fluor with the cell membrane compared to Ru-D-R8. This high concentration at the cell surface could facilitate the non-endocytic uptake mechanism, promoting access to the cytosol and, ultimately, the nucleus, while low concentrations at the cell surface should limit the uptake to endocytosis, with consequent endosomal trapping, observed as punctate cytoplasmic staining.

3.4: CONCLUSIONS

Conjugation of D-octaarginine to $Ru(phen)(bpy')(dppz)^{2+}$ dramatically improves its rate of cellular uptake, reducing the incubation time required to microscopically

observe uptake to less than an hour. At sufficient concentration of conjugate (~ 15 μM), the peptide also increases the nuclear localization; below this threshold concentration only cytoplasmic staining is observed.

This system also allows us to directly observe the effect of a covalently attached fluorescein on cellular uptake properties of the Ru-peptide conjugate. The fluorescein labeled conjugate, Ru-D-R8-fluor, localizes in the nucleus under conditions in which Ru-D-R8 is excluded. Thus, fluorophore tagging of a cell-penetrating peptide does more than supply luminescence. The molecular nature of the organic fluorophore affects the transport pathway and its subcellular localization. Hence, the localization of the fluorophore-bound peptide cannot simply serve as a proxy for that of the free peptide.

3.5: REFERENCES

1. Hart, J. R.; Glebov, O.; Ernst, R. J.; Kirsch, I. L.; Barton, J. K. *Proc. Natl. Acad. Sci. U. S. A.* **2006,** *103*, 15359–15363.
2. Zeglis, B. M; Pierre, V. C.; Barton, J. K. *Chem. Commun.* **2007,** 4565–4579.
3. Ernst, R. J.; Song, H.; Barton, J. K. *J. Am. Chem. Soc.* **2009,** *131*, 2359–2366.
4. Puckett, C. A.; Barton, J. K. *J. Am. Chem. Soc.* **2007,** *129,* 46–47.
5. Stewart, K. M.; Horton, K. L.; Kelley, S. O. *Org. Biomol. Chem.* **2008,** *6,* 2242–2255.
6. Fischer, R.; Fotin-Mleczek, M.; Hufnagel, H.; Brock, R. *ChemBioChem* **2005,** *6,* 2126–2142.
7. Goun, E. A.; Pillow, T. H.; Jones, L. R.; Rothbard, J. B.; Wender, P. A. *ChemBioChem* **2006,** *7,* 1497–1515.
8. Pouton, C. *Adv. Drug Del. Rev.* **1998**, *34*, 51–64.
9. Brunner, J.; Barton, J. K. *Biochemistry* **2006,** *45,* 12295–12302.
10. Fischer, R.; Waizenegger, T.; Köhler, K.; Brock, R. *Biochim. Biophys. Acta* **2002,** *1564,* 365–374.
11. El-Andaloussi, S.; Järver, P.; Johansson, H. J.; Langel, Ü. *Biochem. J.* **2007,** *407,* 285–292.
12. Szeto, H. H.; Schiller, P. W.; Zhao, K.; Luo, G. *FASEB J.* **2005,** *19,* 118–120.
13. Best, T. P.; Edelson, B. S.; Nickols, N. G.; Dervan, P. B. *Proc. Natl. Acad. Sci. U. S. A.* **2003,** *100,* 12063–12068.

14. Edelson, B.; Best, T.; Olenyuk, B.; Nickols, N. Doss, R.; Foister, S.; Heckel, A.; Dervan, P. *Nucleic Acids Res.* **2004,** *32,* 2802–2818.

15. Copeland, K. D.; Lueras, A. M. K.; Stemp, E. D. A.; Barton, J. K. *Biochemistry* **2002,** *41,* 12785–12797.

16. Nakase, I.; Takeuchi, T.; Tanaka, G.; Futaki, S. *Adv. Drug Delivery Rev.* **2008,** *60,* 598–607.

17. Puckett, C. A.; Barton, J. K. *Biochemistry* **2008,** *47,* 11711–11716.

18. Fretz, M. M.; Penning, N. A.; Al-Taei, S.; Futaki, S.; Takeuchi, T.; Nakase, I.; Storm, G.; Jones, A. T. *Biochem. J.* **2007,** *403,* 335–342.

19. Mitchell, D. J.; Kim, D. T.; Steinman, L.; Fathman, C.G.; Rothbard, J. B. *J. Peptide Res*. **2000,** *56,* 318–325.

20. Duchardt, F.; Fotin-Mleczek, M.; Schwarz, H.; Fischer, R.; Brock, R. *Traffic* **2007,** *8,* 848–866.

21. Kosuge, M.; Takeuchi, T.; Nakase, K., Jones, A. T.; Futaki, S. *Bioconjugate Chem.* **2008,** *19,* 656–664.

CHAPTER 4: TARGETING A RUTHENIUM COMPLEX TO THE NUCLEUS WITH SHORT PEPTIDES

4.1: INTRODUCTION

Peptide conjugation is a widely used and effective method for improving both cellular and nuclear entry of a variety of cargo molecules.[1–3] We have successfully delivered our rhodium(III) 5,6-chrysenequinone diimine (chrysi) and ruthenium(II) dipyridophenazine (dppz) complexes to the nucleus through covalent attachment of octaarginine (Chapter 3).[4,5] Without the peptide, these compounds localize in the cytoplasm, as seen by microscopy studies on the luminescent Ru(II) dppz complexes.[6] The chrysi complexes of rhodium(III) bind single base mismatches in DNA,[7,8] but the added +8 charge imparted by octaarginine increases the nonspecific binding of the metal-peptide conjugate, due to electrostatic association with the negatively charged DNA backbone.[4] In order to enhance the nuclear accumulation of our chrysi complexes of rhodium(III) without significant impairment of their specificity for mismatches, we appended shorter peptides possessing less overall charge than octaarginine.

Studies by Kelley and coworkers have demonstrated the feasibility of using very short peptides to target small molecules to the nucleus or mitochondria.[9,10] Thiazole orange (TO) conjugated to the tetrapeptide RrRK (r = D-arginine) accumulates primarily in the nucleus of HeLa cells, whereas TO-FrFK localizes mainly in the mitochondria. Both conjugates are reported to cross the plasma membrane with efficiencies approaching that of the longer Tat peptide (RKKRRQRRR).[9] Using RrRK as the nuclear targeting

signal for our chrysi complexes of rhodium(III) cuts the positive charge added by the peptide in half compared to octaarginine, and thus should reduce the amount of nonspecific DNA binding. Here, we use dppz complexes of Ru(II) functionalized with short peptides, luminescent analogues of our rhodium complexes, to evaluate the cellular uptake.

4.2: EXPERIMENTAL PROTOCOLS

4.2.1: MATERIALS AND INSTRUMENTATION

Media, cell culture supplements, Hanks' Balanced Salt Solution, and TO-PRO®-3 iodide were purchased from Invitrogen (Carlsbad, CA).

MALDI measurements were performed on an Applied Biosystems Voyager 6215. Absorption spectra were recorded on a Beckman DU 7400 spectrophotometer. HPLC was performed on an HP1100 system equipped with a diode array detector using a Vydac C_{18} reversed-phase semipreparative column.

4.2.2: SYNTHESIS OF RU-PEPTIDE CONJUGATES

Peptides, protected and resin-bound, were purchased from Anaspec (Fremont, CA). Rink resin was used to produce amide-terminated peptides. $Ru(phen)(bpy')(dppz)^{2+}$ was coupled to the peptide in an analogous manner to that previously described (where phen = 1,10-phenanthroline, bpy′ = 4-(3-carboxypropyl)-4′-methyl-2,2′-bipyridine, and dppz = dipyrido[3,2-*a*:2′,3′-*c*]phenazine).[4,11] The Ru-RrRK conjugate was synthesized in both the amide- and carboxy-terminated versions for comparison; unless otherwise noted,

Ru-RrRK refers to the amide-terminated form. Ru-KSKKQK and Ru-PKKKRKV were synthesized with C-terminal amides, and Ru-D-R4, Ru-KKKK, and Ru-SrSr have the C-terminal carboxylic acid. Ruthenium-peptide conjugates were purified by reversed-phase HPLC using a water (0.1% trifluoroacetic acid)/acetonitrile gradient and characterized by MALDI-TOF mass spectrometry; Ru-RrRK: 1416.3 *m/z* (M^+) obsd, 1415.6 *m/z* (M^+) calcd, Ru-RrRK-COOH: 1417.6 *m/z* (M^+) obsd, 1416.6 *m/z* (M^+) calcd, Ru-RrRK-fluor: 1935.6 *m/z* (M^+) obsd, 1933.7 *m/z* (M^+) calcd, Ru-D-R4: 1443.6 *m/z* (M^+) obsd, 1444.6 *m/z* (M^+) calcd, Ru-KKKK: 1333.0 *m/z* (M^+) obsd, 1332.6 *m/z* (M^+) calcd, Ru-SrSr: 1307.1 *m/z* (M^+) obsd, 1306.4 *m/z* (M^+) calcd, Ru-PKKKRKV: 1683.8 *m/z* (M^+) obsd, 1683.8 *m/z* (M^+) calcd, Ru-KSKKQK: 1546.6 *m/z* (M^+) obsd, 1546.7 *m/z* (M^+) calcd. All conjugates employed in this study were used as their trifluoroacetate salts. Concentrations were determined by the absorption of $Ru(phen)(bpy')(dppz)^{2+}$; for Ru-RrRK-fluor, 361 nm, which is not obscured by fluorescein, was used (ε_{440}= 19,000 M^{-1} cm^{-1}; ε_{361}= 19,469 M^{-1} cm^{-1}). $Ru(phen)_2dppz^{2+}$, used for comparison to the conjugates in uptake studies, was synthesized as described previously;[6] $\varepsilon_{440\ nm}$ = 21,100 M^{-1} cm^{-1}.[12]

4.2.3: CELL CULTURE

HeLa cells (ATCC, CCL-2) were maintained in minimal essential medium alpha with 10% fetal bovine serum (FBS), 100 units/mL penicillin, and 100 μg/mL streptomycin. Cells were grown in tissue culture flasks at 37 °C under 5% CO_2 atmosphere.

4.2.4: CONFOCAL MICROSCOPY

HeLa were seeded using 4000 cells in wells of a glass-bottom 96-well plate (Whatman, Inc.) and allowed to adhere overnight. The complexes were incubated with HeLa cells at 37 °C in complete medium (minimal essential medium alpha with 10% fetal bovine serum) or medium without serum, as indicated. Imaging was performed using a 63x/1.4 oil immersion objective on a Zeiss LSM 510 or a Zeiss LSM 5 Exciter inverted microscope. The optical slice was set to 1.1 μm. Ru-peptide conjugates were excited at 488 nm, with emission observed at 560+ nm. For Ru-RrRK-fluor, the emission was collected as the combined emission of Ru and fluorescein (505+ nm), both of which are excited at 488 nm. A higher detector gain was necessary to observe the luminescence of Ru-KSKKQK and Ru-PKKKRKV compared to the other conjugates.

4.2.5: FLOW CYTOMETRY

Cells were detached from culture with EDTA (0.48 mM in phosphate-buffered saline) and incubated at $1x10^6$ cells/mL with 10 μM ruthenium complex in Hanks' Balanced Salt Solution (HBSS) supplemented with 2.5 mg/mL bovine serum albumin fraction V (BSAV) at 37 °C for 2 h, then rinsed with buffer and placed on ice. TO-PRO-3 was added at 1 μM immediately prior to flow cytometry analysis to stain dead cells. The fluorescence of ~ 20,000 cells was measured using a BD FACS Aria at the Caltech Flow Cytometry Facility. Ruthenium complexes were excited at 488 nm, with emission observed at 600–620 nm. TO-PRO-3 was excited at 633 nm, with emission observed at

650–670nm. Cells exhibiting TO-PRO-3 fluorescence were excluded from the data analysis.

4.3: RESULTS AND DISCUSSION

4.3.1: SYNTHESIS OF THE CONJUGATES

A series of Ru(II) dipyridophenazine (dppz) conjugates were prepared by solid-phase coupling of $Ru(phen)(bpy')(dppz)^{2+}$ to the N-terminal amine of the peptide. The dppz complexes of ruthenium(II) serve as luminscent analogues of our chrysi complexes of rhodium(III); They function as light switches for non-aqueous environments, luminescing only when bound to the hydrophobic regions of membranes, nucleic acids, and other macromolecules.[13,14] Furthermore, the ruthenium complexes are stable in aqueous solution, making them useful cellular probes.

4.3.2: CELLULAR UPTAKE OF RU-RRRK

We conjugated $Ru(phen)(bpy')(dppz)^{2+}$ to the nuclear targeting signal RrRK (r = D-arginine)(**Figure 4.1**). HeLa cells incubated for 2 h with 5–20 μM Ru-RrRK show punctate cytoplasmic luminescence, but no staining of the nucleus (**Figure 4.2**). Interestingly, increasing the incubation time to 24 h does not change the subcellular localization of 20 μM Ru-RrRK. This staining pattern is similar to that previously observed for the D-octaarginine conjugate of this ruthenium complex (Ru-D-R8) at 5–10 μM.[5] This distribution also implicates endocytosis, a proposed mechanism of uptake for oligoarginine cell penetrating peptides,[15] as the mode of entry; though, this remains to

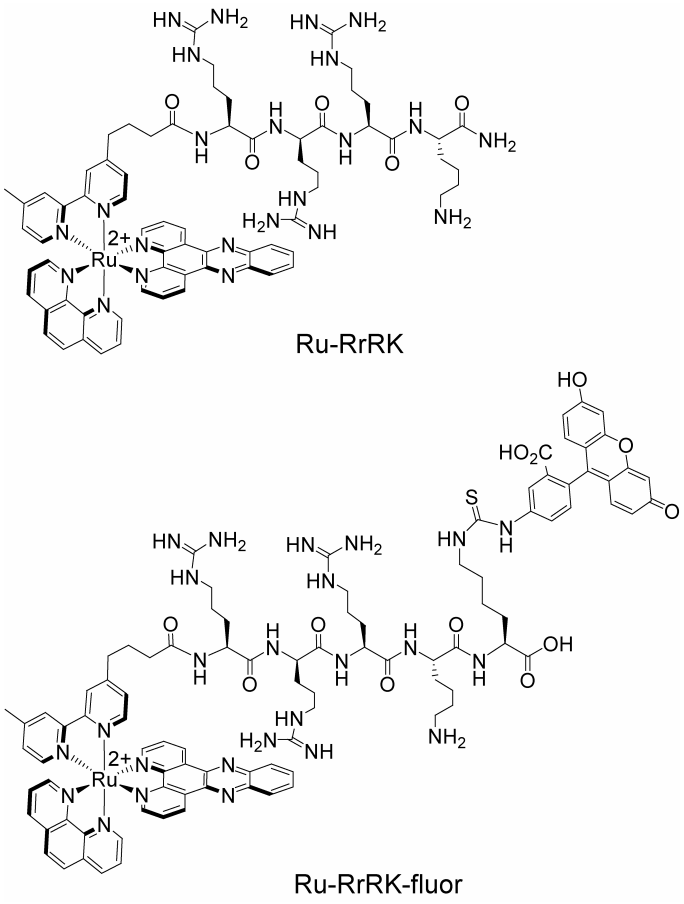

Figure 4.1: Structures of Ru-RrRK conjugates.

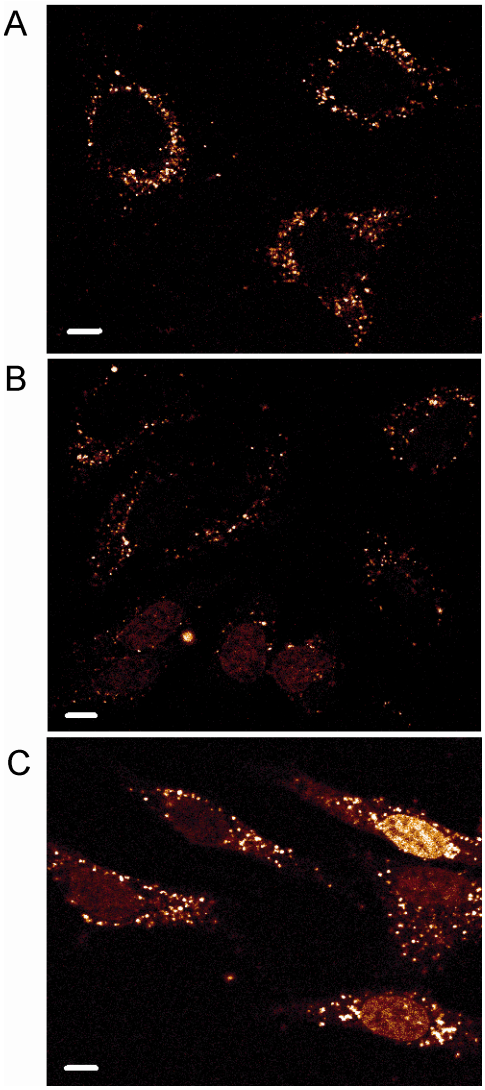

Figure 4.2: Subcellular distribution of Ru-RrRK. HeLa were incubated with (A) 20, (B) 40, or (C) 100 μM Ru-RrRK in complete medium for 2 h. At 20 μM, only punctate staining of the cytoplasm is present. At higher concentrations, some cells show additional nuclear staining. Scale bars are 10 μm.

be confirmed by mechanistic studies. As expected, cellular uptake of the peptide conjugate is enhanced compared to the unconjugated complex $Ru(phen)_2dppz^{2+}$, as observed by direct comparison of the two complexes by confocal microscopy following identical incubation conditions (10 μM, 2 h). The same enhancement is seen by flow cytometry analysis; cells treated with Ru-RrRK have a 1.7-fold increase in mean luminescence compared to those exposed to $Ru(phen)_2dppz^{2+}$. Note that the luminescence of Ru-RrRK is inherently 60% of $Ru(phen)_2dppz^{2+}$, when measured with calf thymus DNA. In contrast, cellular uptake of Ru-RrRK is a quarter of that for Ru-D-R8 (**Table 4.1**), consistent with previous observations that short oligoarginines are less effective at promoting the cellular entry of fluorescein than longer ones.[16]

There is evidence in the literature that fluorescein-conjugated cell-penetrating peptides can adhere to the cellular exterior,[17] artificially increasing the apparent uptake when measured by flow cytometry. Although trypsinization is recommended to reduce the membrane-bound material, we did not use trypsin in these experiments as it would preferentially cleave at the L-amino acids, thus increasing the apparent amount of Ru-D-R8 cellular uptake versus our other conjugates. Furthermore, the lack of defined staining of the cellular periphery in our confocal microscopy experiments indicates that either our conjugates do not accumulate at the membrane, or that the luminescence of such bound species is quenched.

At higher concentrations, the distribution of Ru-RrRK changes and the cell population becomes heterogeneous. In addition to the punctate cytoplasmic structures, the complex localizes in the nucleus in a small percentage of cells when incubated at

Table 4.1: Cellular uptake of ruthenium conjugates assayed by flow cytometry

complex	mean luminescence[a]
$Ru(phen)_2dppz^{2+}$	79 ± 17
Ru-D-R8	328 ± 11
Ru-RrRK	133 ± 7
Ru-PKKKRKV	86 ± 4
Ru-KSKKQK	73 ± 8

[a]HeLa cells were incubated with 10 μM ruthenium conjugate for 2 h at 37 °C. Ruthenium complexes were excited at 488 nm,with emission observed at 600–620 nm. The mean luminescence intensity of cells not treated with complex is 20. Each data point is the mean ± the standard deviation of three samples.

30–40 μM (**Figure 4.2**). The fraction of cells with nuclear staining increases with concentration of the complex. At 100 μM, the complex is located in the nucleus in 74% of cells (**Table 4.2**).

This population heterogeneity has been observed previously for fluorescein-nonaarginine[18,19] and for our ruthenium-octaarginine conjugate lacking fluorescein (Chapter 3).[5] A notable difference is that Ru-RrRK requires a higher concentration (30 μM versus 15 μM) to accumulate inside the nucleus than Ru-D-R8, and a greater amount (> 40 μM versus 20 μM) is necessary for the majority of cells to exhibit nuclear staining. RrRK is a less effective at promoting nuclear uptake of our ruthenium complex than D-octaarginine.

A shortened oligoarginine, Ru-tetraarginine (Ru-D-R4) was also examined, and it was found to have similar cellular uptake characteristics to Ru-RrRK. When incubated at 20 μM for 2 h, Ru-D-R4 is limited to punctate structures in the cytoplasm (**Figure 4.3**). At 30 μM, no cells had nuclear staining, in contrast to Ru-RrRK which reached the nucleus in 7% of cells. These two conjugates were synthesized with different C-termini, an amide for Ru-RrRK and a carboxylic acid for Ru-D-R4. This could play a small role in their differences in cellular internalization, however the amide- and carboxy-terminated versions of Ru-RrRK at 20 μM and 24 h show similar uptake.

We also evaluated the cellular accumulation of Ru-RrRK in serum-free medium, to allow comparison to the previously described experiments on the thiazole-orange conjugate (TO-RrRK), which were performed in the absence of serum.[9] Not surprisingly, Ru-RrRK enters cells more readily under these conditions, and the concentration required

Table 4.2: Percentage of cells with nuclear staining by Ru-RrRK[a]

concentration (μM)	+serum	-serum
10	0%	0%
20	0%	2%
30	7%	53%
40	14%	65%
100	74%	n.d.

[a]HeLa cells were incubated with Ru conjugate for 2 h at 37 °C in medium +/- serum, then rinsed with HBSS and analyzed by confocal microscopy. Dead cells were excluded by their morphology. Data not determined are indicated by n.d.

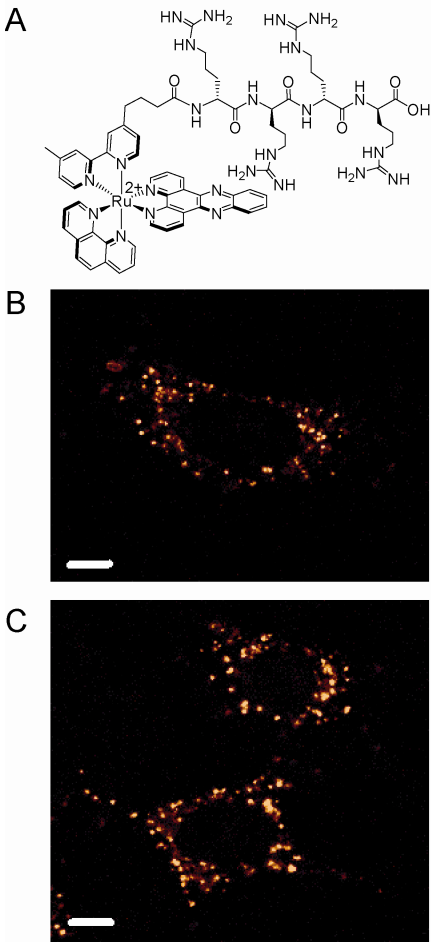

Figure 4.3: Subcellular distribution of Ru-D-R4. The structure of the conjugate is shown in (A). HeLa cells were incubated with (B) 20 or (C) 30 μM Ru-D-R4 in complete medium for 2 h. Punctate staining of the cytoplasm is observed. Scale bars are 10 μm.

for nuclear staining is reduced. At 30 μM complex for 2 h, half of the cells show nuclear staining (**Figure 4.4**, **Table 4.2**). However, Ru-RrRK exhibits less efficient nuclear entry than TO-RrRK, which localizes in the nucleus at a lower incubation concentration (5 μM for 1.5 h) in the same cell line.[9] Hence, the ability of RrRK to impart nuclear localization is affected by the nature of the cargo, with the larger and more positively charged ruthenium complex being more difficult to direct than thiazole orange.

In earlier experiments, we observed that attachment of fluorescein to Ru-D-R8 influences its subcellular distribution, allowing the conjugate with fluorescein to enter the nucleus under conditions for which the complex without fluorescein is excluded.[5] Interestingly, an appended fluoresscein does not have the same effect on Ru-RrRK; instead, cellular uptake is impaired by the dye. At concentrations up to 30 μM and 2 h incubation, only punctate cytoplasmic luminescence is seen (**Figure 4.5**). The lack of benefit from fluorescein could be due the stronger relative effect of its negative charge on this shorter peptide. With reduced positive charge, the conjugate is less able to use the membrane potential as a driving force for entry; membrane potential has been shown to be an important factor in the cellular uptake of guanidinium-rich peptides.[20]

4.3.3: Effect of sequence variations on short peptides

It is known in the literature that charge is not the sole determinant in the uptake of cell-penetrating peptides; oligoarginines enter cells much more effectively than oligolysines.[18] To confirm this for our system, we observed the cellular entry of Ru-KKKK. We also synthesized Ru-SrSr, which has even less charge, but contains two

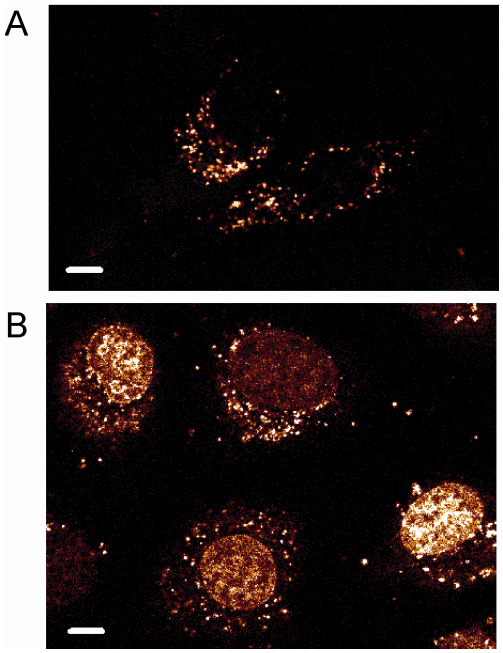

Figure 4.4: Subcellular distribution of Ru-RrRK in serum-free medium. HeLa were incubated with (A) 20 or (B) 40 μM Ru-RrRK in for 2 h. At 20 μM in medium without serum, the most cells show only punctate cytoplasmic staining, while at 40 μM, the majority of cells exhibit additional nuclear labeling. Scale bars are 10 μm.

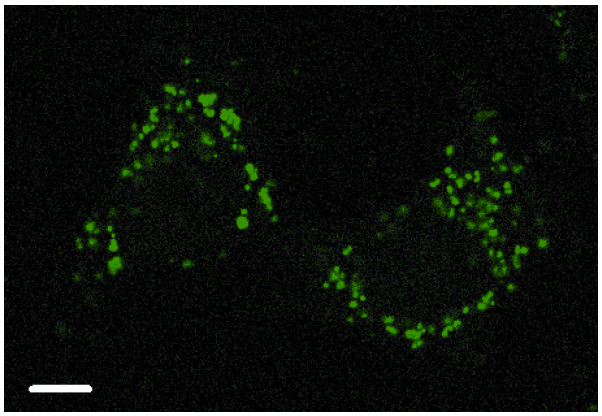

Figure 4.5: Subcellular distribution of Ru-RrRK-fluor. HeLa were incubated with 30 μM Ru-RrRK-fluor for 2 h in complete medium. Punctate staining of the cytoplasm is observed. Scale bar is 10 μm.

arginines. For Ru-KKKK and Ru-SrSr, only faint luminescence in the cytoplasm was observed after incubation at 40 μM for 2 h. Increasing the incubation concentration and time (100 μM, 4 h) leads to brighter, punctate cytoplasmic staining, and a small percentage of cells (17% for Ru-KKKK and 5% for Ru-SrSr) exhibit additional nuclear staining (**Figure 4.6**). Ru-KKKK luminescence is a little more intense than Ru-SrSr, indicating that its increased positive charge gives a small advantage over the two arginines of Ru-SrSr. As expected, both Ru-KKKK and Ru-SrSr are poorly internalized compared to Ru-RrRK.

Two longer peptides that correspond to known nuclear localization signals (NLSs) were also studied, PKKKRKV and KSKKQK.[21] NLSs promote active transport through the nuclear pore complex, but the use of an NLS does not guarantee nuclear uptake. They must reach the cytosol in order to access the nuclear import machinery. If the NLS conjugates enter by endocytosis, they could become trapped in endosomes. However, a cobaltocenium cation has previously been successfully targeted to the nucleus using PKKKRKV.[22] Furthermore, the chosen peptides possess less overall charge than octaarginine, and thus are suitable candidates in our efforts to reduce the nonspecific binding of our metal-peptide conjugates to DNA.

Treatment of HeLa cells with 10 μM Ru-PKKKRKV or Ru-KSKKQK for 2 h reveals faint punctate luminescence in the cytoplasm and no nuclear staining. Increasing the incubation time to 19 h provides the same result (**Figure 4.7**). Hence, neither NLS is better at promoting nuclear localization of our ruthenium complex than D-octaarginine,

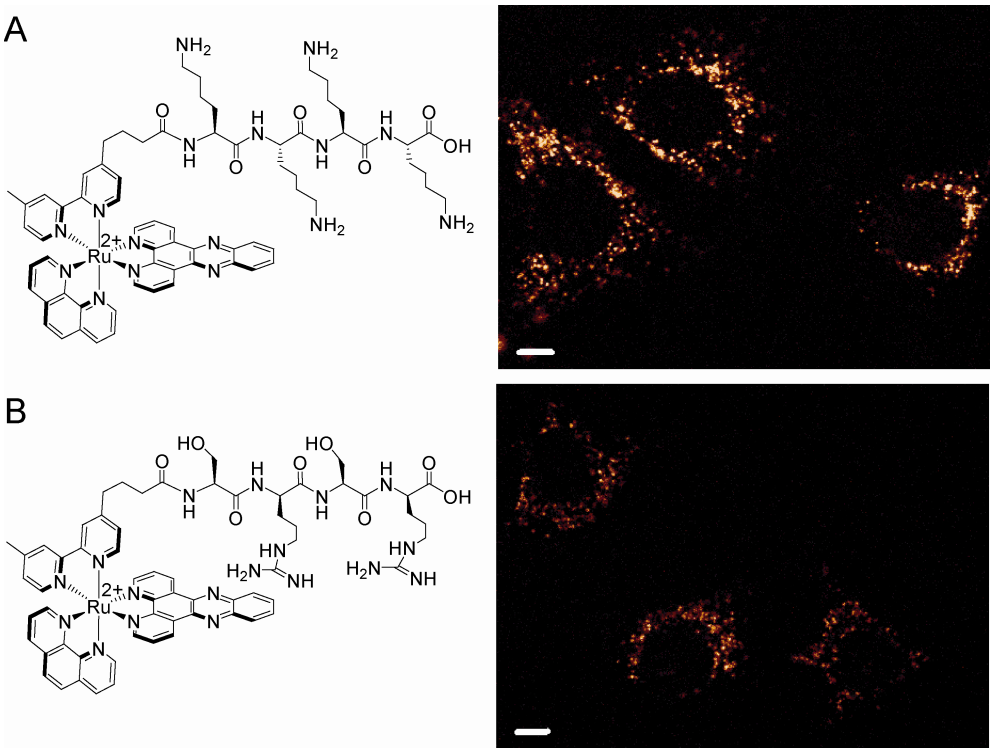

Figure 4.6: Subcellular distribution of Ru-KKKK and Ru-SrSr. HeLa cells were incubated for 4 h with 100 μM (A) Ru-KKKK or (B) Ru-SrSr in complete medium. Structures of the conjugates are shown at left. The cells shown display punctate staining of the cytoplasm. Scale bars are 10 μm.

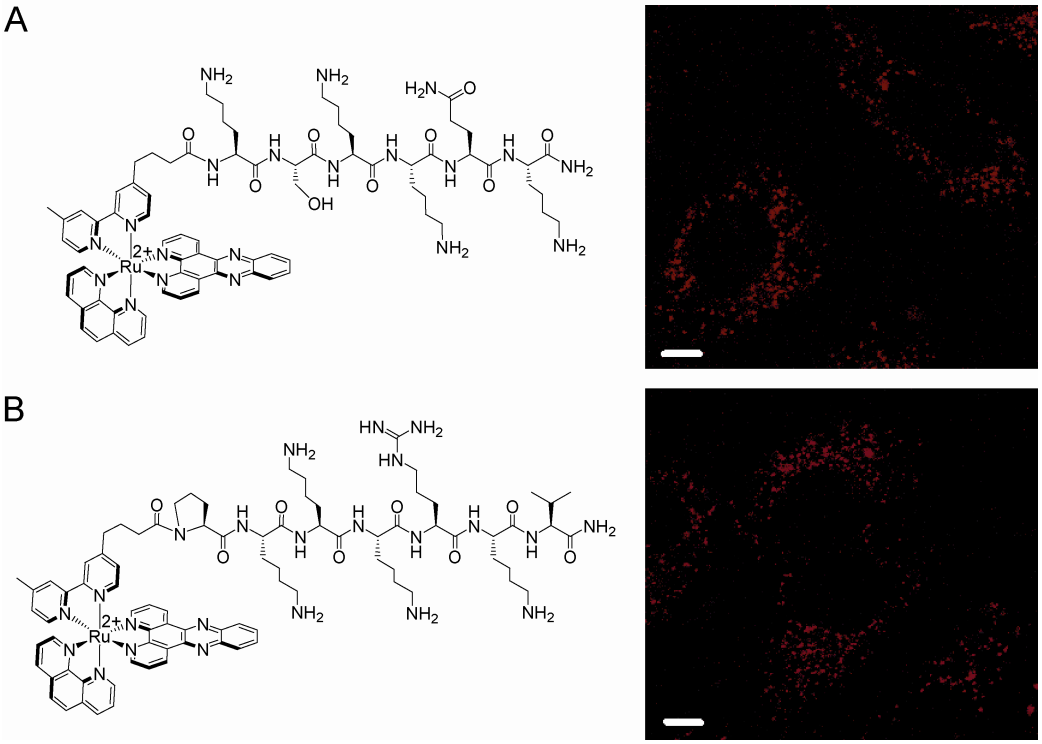

Figure 4.7: Subcellular distribution of Ru-NLS conjugates. HeLa cells were incubated for 19 h with 10 μM (A) Ru-KSKKQK or (B) Ru-PKKKRKV in complete medium. Structures of the conjugates are shown at left. Punctate staining of the cytoplasm is observed. Scale bars are 10 μm.

which is also excluded from the nucleus at 10 μM. In fact, analysis by flow cytometry reveals that cellular accumulation is even less than that for Ru-RrRK, despite having similar charge (**Table 4.1**). Presumably, at higher concentrations, these Ru-NLS conjugates will accumulate in the nucleus, similar to Ru-RrRK. Without measurement of this threshold concentration, we cannot compare their ability as nuclear delivery vectors to RrRK.

4.4: CONCLUSIONS

The large positive charge of octaarginine-metal complex conjugates both improves uptake and interferes with selective DNA-binding. To resolve this issue, we studied our luminescent ruthenium complex tethered to the shorter and less charged RrRK, which efficiently addresses the organic fluorophore thiazole orange to the nucleus.[9] We found that this peptide was far less capable for delivery of the ruthenium complex than it was for thiazole orange, further demonstrating the importance of payload to the accumulation and distribution of cell-penetrating peptides. Furthermore, the low positive charge of short peptide conjugates abrogates the benefits from fluorescein attachment that we previously observed for Ru-octaarginine. Nevertheless, RrRK conjugation increases cellular uptake as compared to analogous unconjugated complexes, and, above a threshold concentration of 30 μM, this peptide targets the ruthenium complex to the nucleus.

4.5: REFERENCES

1. Stewart, K. M.; Horton, K. L.; Kelley, S. O. *Org. Biomol. Chem.* **2008,** *6,* 2242–2255.
2. Fischer, R.; Fotin-Mleczek, M.; Hufnagel, H.; Brock, R. *ChemBioChem* **2005,** *6,* 2126–2142.
3. Goun, E. A.; Pillow, T. H.; Jones, L. R.; Rothbard, J. B.; Wender, P. A. *ChemBioChem* **2006,** *7,* 1497–1515.
4. Brunner, J.; Barton, J. K. *Biochemistry* **2006,** *45,* 12295–12302.
5. Puckett, C. A.; Barton, J. K. *J. Am. Chem. Soc.* **2009,** *131,* 8738–8739.
6. Puckett, C. A.; Barton, J. K. *J. Am. Chem. Soc.* **2007,** *129,* 46–47.
7. Zeglis, B. M; Pierre, V. C.; Barton, J. K. *Chem. Commun.* **2007**, 4565–4579.
8. Ernst, R. J.; Song, H.; Barton, J. K. *J. Am. Chem. Soc.* **2009**, *131*, 2359–2366.
9. Mahon, K.; Potocky, T.; Blair, D.; Roy, M.; Stewart, K.; Chiles, T.; Kelley, S. *Chem. Biol.* **2007,** *14,* 923–930.
10. Horton, K. L.; Steward, K. M.; Fonseca, S. B.; Guo, Q.; Kelley, S. O. *Chem. Biol.* **2008,** *15,* 375–382.
11. Copeland, K. D.; Lueras, A. M. K.; Stemp, E. D. A.; Barton, J. K. *Biochemistry* **2002,** *41,* 12785–12797.
12. Holmlin, R. E.; Stemp, E. D. A.; Barton, J. K. *Inorg. Chem.* **1998,** *37*, 29–34.
13. Friedman, A. E.; Chambron, J.-C.; Sauvage, J.-P.; Turro, N. J.; Barton, J. K. *J. Am. Chem. Soc.* **1990,** *112,* 4960–4962.

14. Jenkins, Y.; Friedman, A. E.; Turro, N. J.; Barton, J. K. *Biochemistry* **1992,** *31,* 10809–10816.

15. Nakase, I.; Takeuchi, T.; Tanaka, G.; Futaki, S. *Adv. Drug Delivery Rev.* **2008,** *60,* 598–607.

16. Wender, P. A.; Mitchell, D. J.; Pattabiraman, K.; Pelkey, E. T.; Steinman, L.; Rothbard, J. B. *Proc. Natl. Acad. Sci. U. S. A.* **2000,** *97,* 13003–13008.

17. Richard, J. P.; Melikov, K.; Vives, E.; Ramos, C.; Verbeure, B.; Gait, M. J.; Chernomordik, L. V.; Lebleu, B. *J. Biol. Chem.* **2003,** *278,* 585–590.

18. Mitchell, D. J.; Kim, D. T.; Steinman, L.; Fathman, C.G.; Rothbard, J. B. *J. Peptide Res*. **2000,** *56,* 318–325.

19. Duchardt, F.; Fotin-Mleczek, M.; Schwarz, H.; Fischer, R.; Brock, R. *Traffic* **2007,** *8,* 848–866.

20. Rothbard, J. B.; Jessop, T. C.; Lewis, R. S.; Murray, B. A.; Wender, P. A. *J. Am. Chem. Soc.* **2004,** *126,* 9506–9507

21. Pouton, C. *Adv. Drug Del. Rev.* **1998,** *34*, 51–64.

22. Noor, F.; Wustholz, A.; Kinscherf, R.; Nolte, N. *Angew. Chem. Int. Ed.* **2005,** *44,* 2429–2432.

CHAPTER 5: CONCLUSIONS

The cellular uptake of transition metal complexes is only beginning to be explored, despite their potential utilization for biological applications. Here, we have demonstrated that luminescent dipyridophenazine (dppz) complexes of ruthenium(II) are well suited for studies of internalization and distribution in living cells. Using flow cytometry and confocal microscopy, we have systematically examined the effect of ancillary ligand variation on their cellular uptake. Lipophilicity is the strongest structural determinant for uptake efficiency, with the greatest internalization observed for $Ru(DIP)_2dppz^{2+}$, where DIP = 4,7-diphenyl-1,10-phenanthroline. This complex enters cells *via* passive diffusion, driven by the plasma membrane potential, as determined by a series of mechanistic studies. Furthermore, the dependence of cellular accumulation on lipophilicity is consistent with passive diffusion being the common mechanism of entry for the entire family. Surprisingly, although the nuclear pore complex is purported to be permeable to small molecules, nuclear accumulation of these complexes is relatively poor under conditions where they are present in the cytoplasm.

The dipyridophenazine complexes of ruthenium(II) furthermore serve as luminescent analogues of our 5,6-chrysenequinone diimine (chrysi) complexes of rhodium(III), which we are exploring as potential chemotherapeutic agents. These rhodium complexes target single base mismatches in DNA and selectively inhibit cellular proliferation in mismatch repair-deficient cell lines. Importantly, the biological activity of these complexes has been demonstrated to be a consequence of their DNA-binding,

suggesting that they reach the nucleus.[1,2] Naturally, we have a strong interest in understanding the uptake of these complexes, and optimizing their structure for the uptake and distribution properties that maximize therapeutic function. However, larger, more lipophilic complexes, although more readily internalized, interfere with DNA-binding, and hence biological activity.[2] As a result, we explored peptide conjugates, which we hypothesized should enter cells readily, without need of lipophilic bulk added near the metal.

Conjugation of D-octaarginine to $Ru(phen)(bpy')(dppz)^{2+}$ dramatically improves its rate of cellular uptake. At sufficient concentration of conjugate (~ 15 μM), the peptide also increases the nuclear localization; below this threshold concentration only cytoplasmic staining is observed. However, the uptake properties of the peptide are not independent of its payload. This is well demonstrated by the effects of tethering fluorescein to the metal-peptide conjugate. This doubly labeled peptide has a lower threshold concentration: the conjugate strongly stains the nucleus under conditions for which the construct without fluorescein is excluded. Furthermore, appending octaarginine to the rhodium complex increases the nonspecific affinity for DNA, decreasing the selectivity for mismatches.[3] We attempted to attenuate this effect by employing, shorter, less charged peptides, but found in each case that a much higher threshold concentration was required for nuclear entry. Hence, peptide conjugation as a strategy for nuclear delivery is subject to the same challenge as we demonstrated for the lipophilic complexes: structural variation for the optimization of uptake and distribution invariably affects functional properties, while the reverse is also true.

To avoid this complication, we are exploring strategies to allow optimization of the nuclear targeting moiety without affecting the activity of the complex. Current efforts involve separation of the uptake moiety from the payload with cleavable linkers. Ideally, these will release the active compound upon delivery to the target.

REFERENCES

1. Hart, J. R.; Glebov, O.; Ernst, R. J.; Kirsch, I. R.; Barton, J. K. *Proc. Natl. Acad. Sci. U. S. A.* **2006,** *103*, 15359–15363.

2. Ernst, R. J.; Song, H.; Barton, J. K. *J. Am. Chem. Soc.* **2009**, *131*, 2359–2366.

3. Brunner, J.; Barton, J. K. *Biochemistry* **2006**, *45*, 12295–12296.

APPENDIX: SYNTHESIS OF A LONG-LIFETIME BINARY MOLECULAR BEACON[§]

A1.1: INTRODUCTION

Ruthenium complexes possess long luminescent lifetimes (~ 1 μs). When the Ru complex functions as the donor in a resonance energy transfer (RET) pair, its long lifetime is inherited by the RET acceptor. Here, we describe the synthesis of a long-lifetime molecular beacon consisting of two probes: (1) $Ru(DIP)_2(bpy')^{2+}$ (where bpy′= 4-(3-carboxypropyl)-4′-methyl-2,2′-bipyridine) tethered to the 3′ end of a DNA oligonucleotide and (2) the organic fluorophore Cy5 tethered to the 5′ end of a DNA oligonucleotide. The two strands are complementary to adjacent regions of the target. In the presence of target DNA or RNA, the two fluorophores are brought together and energy transfer between Ru and Cy5 occurs (**Figure A1.1**). Described elsewhere, detection by these probes was studied by time-resolved emission measurements, and the luminescence in the presence of target is temporally well distinguished from the intense, but shorter-lived autofluorescence of cellular media.[1]

A1.2: EXPERIMENTAL PROTOCOLS

A1.2.1: PROBE SEQUENCE

The probe sequences are complementary to a region of *Aplysia californica* sensorin mRNA. A region low in secondary structure was selected as the target for the

---

[§] Adapted from the supporting information to Martí, A. A.; Puckett, C. A.; Dyer, J.; Stevens, N.; Jockusch, S.; Ju, J.; Barton, J. K.; Turro, N. J. Inorganic-organic hybrid luminescent binary probe for DNA detection based on spin-forbidden resonance energy transfer. *J. Am. Chem. Soc.* **2007,** *129,* 8680–8681.

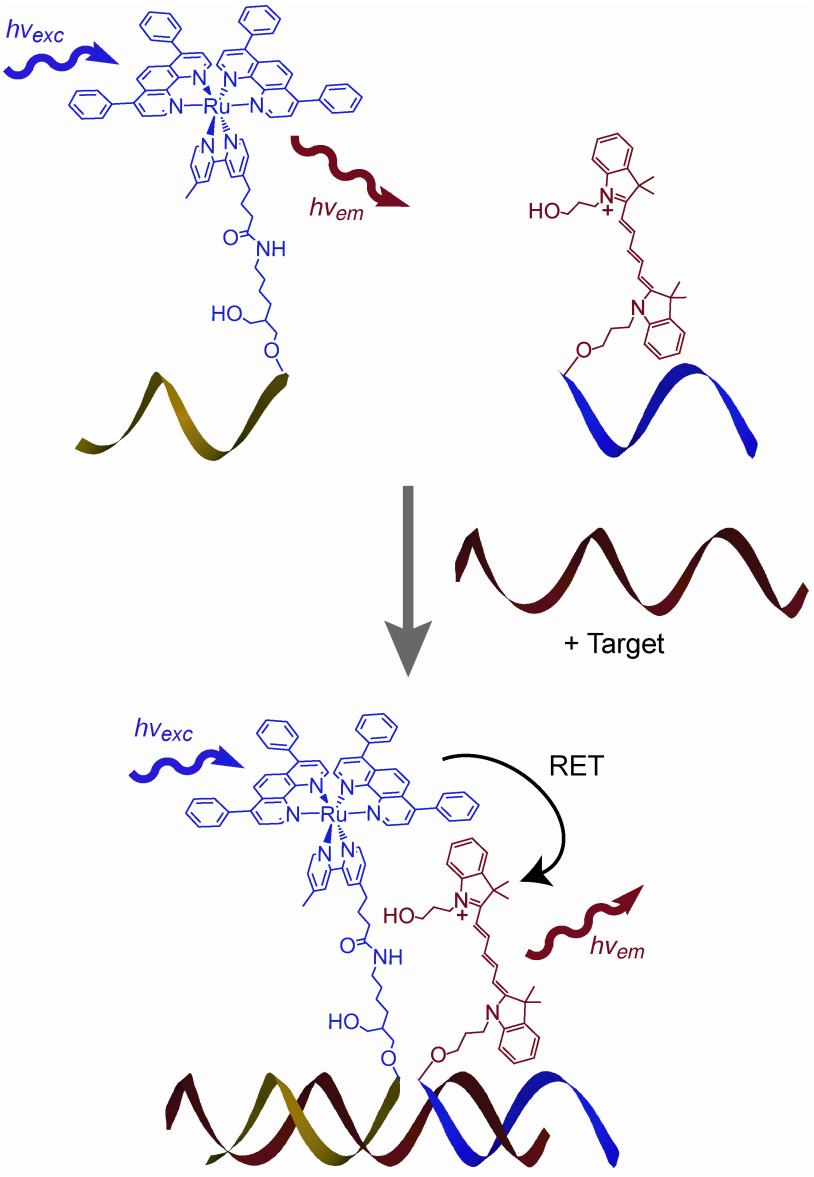

Figure A1.1: Detection of DNA by a binary molecular beacon. When the probes are free in solution, only emission from the ruthenium complex is observed. In the presence of target, $Ru(DIP)_2(bpy')^{2+}$ and Cy5 are brought into close proximity, a condition favorable for resonance energy transfer (RET), and mainly Cy5 emission is observed.

binary probe based on the modeled secondary structure. The modeling details have been reported elsewhere.[2]

Ru-probe: 5′-AAG TTG ATC AAG TTG GT-($Ru(DIP)_2(bpy')^{2+}$)-3′

Cy5-Probe-1: 5′-Cy5-TAT GTT TCA CTG GAT GA-3′

Cy5-Probe-2: 5′-Cy5-ATG TTT CAC TGG ATG A-3′

Cy5-Probe-3: 5′-Cy5-TTC ACT GGA TGA-3′

Target: 5′-TCA TCC AGT GAA ACA TAC AGC ACC AAC TTG ATC AAC TT-3′

A1.2.2: PROBE SYNTHESIS

A1.2.2.1: SYNTHESIS OF $[Ru(DIP)_2(bpy')]Cl_2$

$Ru(DIP)_2Cl_2$ was synthesized in analogous fashion to the published synthesis of $Ru(bpy)_2Cl_2$.[3] $Ru(DIP)_2(bpy')^{2+}$ was prepared by refluxing 41 mg of $Ru(DIP)_2Cl_2$ (49 μmol) and 16.4 mg (64 μmol) of 4-(3-carboxypropyl)-4′-methyl-2,2′-bipyridine (prepared according to the published procedure)[4] in 10 mL of 1:1 ethanol:water for 3 h. The mixture was cooled to ambient temperature and the ethanol removed *in vacuo*. The solution was diluted with water (20 mL) and filtered. The complex was precipitated as the PF_6^- salt by addition of NH_4PF_6, then returned to the Cl^- salt using a Sephadex DEAE anion exchange column. ESI-MS (cation): 511.3 *m/z* (M^{2+}) obsd, 511.1 *m/z* (M^{2+}) calcd. $\varepsilon_{440} = 35{,}200\ M^{-1}\ cm^{-1}$ in water, as determined by inductively coupled plasma mass spectrometry (ICP-MS) measurements.

A1.2.2.2: SYNTHESIS OF THE RU-PROBE

$Ru(DIP)_2(bpy')^{2+}$ was tethered to the 3′-end of DNA by first coupling the complex to amine-modified beads, followed by DNA synthesis and cleavage of the Ru-DNA conjugate from the beads (**Figure A1.2**).[5] The Fmoc group was removed from 3′-amino-modifier C7 CPG 500 beads (Glen Research) by incubation with 20% piperidine in DMF for 15 min. The beads were rinsed with DMF and CH_3CN, dried *in vacuo*, then placed under $Ar_{(g)}$. To the beads (2 μmol), $[Ru(DIP)_2(bpy')]Cl_2$ (4.5 mg, 4 μmol), HBTU (1.5 mg, 4 μmol), HOBT (0.6 mg, 4 μmol), and DIEA (2 μL, 12 μmol) in anhydrous DMF (1.5 mL) were added. The reaction mixture was shaken for 30 min at ambient temperature. The beads were rinsed with DMF, CH_3CN, and CH_2Cl_2, then divided into two aliquots and transferred into two DNA synthesis columns. DNA was synthesized using an ABI 3400 DNA synthesizer. The DNA was cleaved from the beads and deprotected with conc. NH_4OH (2 h at ambient temperature, 6 h at 60 °C). The Ru-DNA conjugate was purified by HPLC using a gradient of 5:95 to 65:35 (acetonitrile:50 mM ammonium acetate) over 30 min. The DMT was removed with 80% acetic acid for 15 min, followed by addition of ethanol, and removal of solvent *in vacuo*. The Ru-DNA conjugate was purified once more by HPLC. MALDI-TOF: 6473 *m/z* (M^+) obsd, 6477 *m/z* (M^+) calcd.

A2.2.2.3: SYNTHESIS OF THE CY5-PROBES

DNA was synthesized using ‘ultramild’ reagents with Cy5 was added at the 5′-end, using a Cy5 phosphoramidite (Glen Research). The MMT group was removed by

the DNA synthesizer. The DNA was cleaved and deprotected with 0.05 M potassium carbonate in methanol for 4 h at ambient temperature. To the supernatant, 1.5 equivalents by volume 2.0 M TEAA were added. The solution was concentrated *in vacuo* and desalted using a Nap10 column (GE Healthcare), eluting with water. The Cy5-DNA conjugate was purified by HPLC using a gradient of 5:95 to 65:35 (acetonitrile:50 mM ammonium acetate) over 30 min. MALDI-TOF: Cy5-Probe-1, 5748 *m/z* (M^+) obsd, 5749 *m/z* (M^+) calcd; Cy5-Probe-2, 5442 *m/z* (M^+) obsd, 5445 *m/z* (M^+) calcd; Cy5-Probe-3, 4193 *m/z* (M^+) obsd, 4194 *m/z* (M^+) calcd.

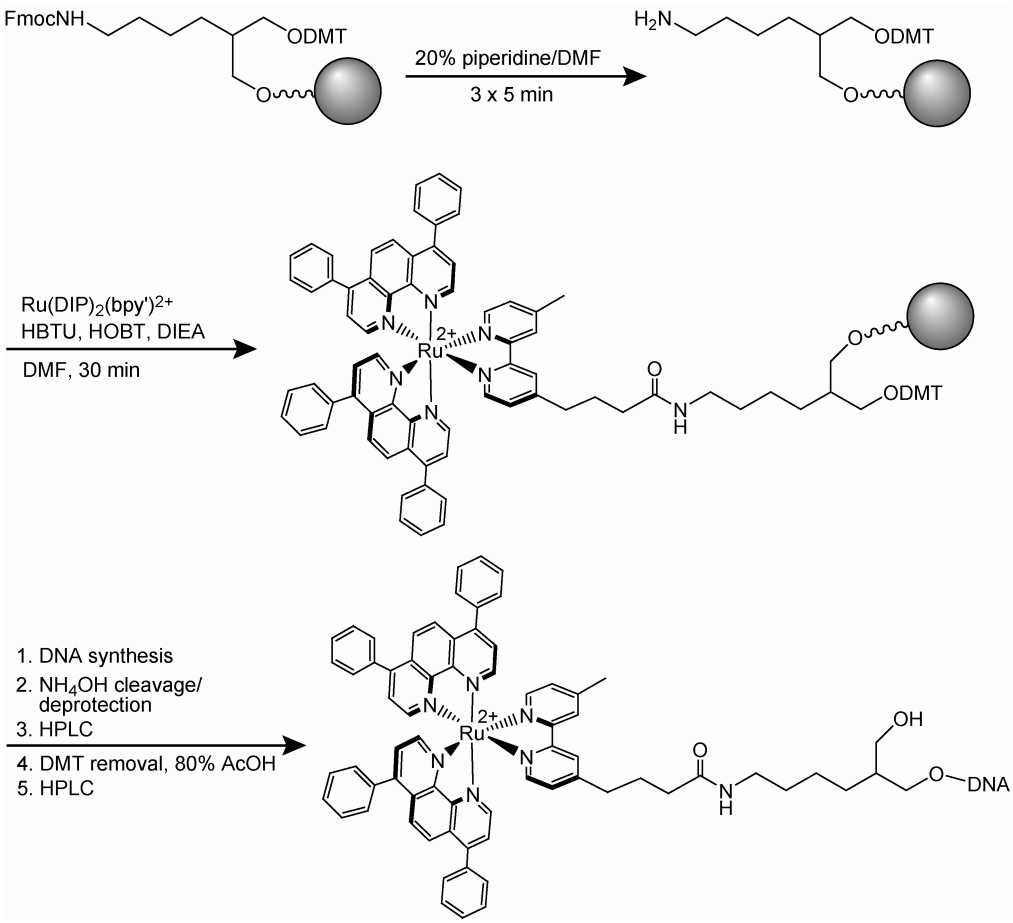

Figure A1.2: Synthesis of the Ru-probe.

A1.3: REFERENCES

1. Martí, A. A.; Puckett, C. A.; Dyer, J.; Stevens, N.; Jockusch, S.; Ju, J.; Barton, J. K.; Turro, N. J. *J. Am. Chem. Soc.* **2007,** *129,* 8680–8681.
2. Martí, A. A.; Li, X.; Jockusch, S.; Li, Z.; Raveendra, B.; Kalachikov, S.; Russo, J. J.; Morozova, I.; Puthanveettil, S. V.; Ju, J.; Turro, N. J. *Nucleic Acids Res.* **2006**, *34*, 3161–3168.
3. Sullivan, B. P.; Salmon, D. J.; Meyer, T. J. *Inorg. Chem.* **1978**, *17*, 3334–3341.
4. Della Ciana, L.; Hamachi, I.; Meyer, T. J. *J. Org. Chem.* **1989**, *54*, 1731–1735.
5. Holmlin, R. E.; Dandliker, P. J.; Barton, J. K. *Bioconjugate Chem.* **1999**, *10*, 1122–1130.